IEEE Access
Multidisciplinary ⋮ Rapid Review ⋮ Open Access Journal

Received November 26, 2021, accepted November 30, 2021, date of publication December 6, 2021,
date of current version December 24, 2021.

Digital Object Identifier 10.1109/ACCESS.2021.3133285

Artificial Intelligence-Based Power System Stabilizers for Frequency Stability Enhancement in Multi-Machine Power Systems

ALIYU SABO[1], (Student Member, IEEE), NOOR IZZRI ABDUL WAHAB[1], (Senior Member, IEEE), MOHAMMAD LUTFI OTHMAN[1], (Senior Member, IEEE), MAI ZURWATUL AHLAM BINTI MOHD JAFFAR[2], HAKAN ACIKGOZ[3], HAMED NAFISI[4], AND HOSSEIN SHAHINZADEH[5], (Member, IEEE)

[1]Advanced Lightning, Power and Energy Research (ALPER), Department of Electrical and Electronics Engineering, University Putra Malaysia (UPM), Serdang, Selangor 43400, Malaysia
[2]Department of Mathematics, Faculty of Science, University Putra Malaysia (UPM), Serdang, Selangor 43400, Malaysia
[3]Department of Electrical Electronics Engineering, Faculty of Engineering and Natural Sciences, Gaziantep Islam Science and Technology University, 27010 Gaziantep, Turkey
[4]School of Electrical and Electronic Engineering, Technological University Dublin (TU Dublin), Dublin 7, D07 EWV4 Ireland
[5]Department of Electrical Engineering, Amirkabir University of Technology (Tehran Polytechnic), Tehran 1591634311, Iran

Corresponding authors: Aliyu Sabo (saboaliyu98@gmail.com), Hamed Nafisi (hamed.nafisi@tudublin.ie), and Noor Izzri Abdul Wahab (izzri@upm.edu.my)

This work was supported by the Geran Putra Berimpak (GPB)-UPM, University Putra Malaysia, Selangor, Malaysia, under Grant 9630000.

ABSTRACT Low frequency oscillations (LFOs) occur in a system of interconnected generators connected by weak interconnection. A power system stabilizer (PSS) is commonly used to improve the capacity of the power system dampening. Under a variety of operating conditions, traditional PSSs fail to deliver superior damping. To address this issue, a Farmland Fertility Algorithm (FFA-PSSs controller) was used to solve an optimization problem for optimal design of PSSs system parameters, and its performance efficiency was compared to GA and PSO-based PSSs controllers. In addition to PSS, flexible current transmission (FACTS) devices are widely used. PSSs controllers and FACTS devices are frequently constructed in tandem to improve the dampening efficiency of the system. In this study, an Interline Power Flow Controller (IPFC) FACTS device will be added to the PSSs controller to improve the power system's oscillatory stability. PSSs optimal design and supplemental controller of power fluctuations for IPFC were conducted out on WSCC multi-machine test systems using a system linear model. Using time-domain simulations and quantitative analysis, the proposed IPFC model was compared to the FFA-PSSs controller in terms of performance and efficiency. The main disadvantage of this technique is the difficulty in designing a dynamic IPFC model in test systems, as well as the burden of IPFC coordinated PSSs optimization. In both PSSs design using FFA method and FFA-optimized PSS with IPFC cases, rise in the computational and simulation costs was found unavoidable. To compensate for these flaws and obtain the research contribution, this paper proposes a Neuro-Fuzzy Controller (NFC) developed as a damping controller that can take the place of the two controllers (research objectives three). The application of the NFC substitute the computational and simulation cost involved in designing multi-machine PSS and IPFC-FACTS systems simultaneously. With the availability of NFC in SIMULINK, a dynamic model of the WSCC three-machine system was developed under a variety of operating situations. Quantitative analysis results from the WSCC test system simulation show that when comparing the proposed NFC model to the IPFC model for the WSCC test system, the proposed NFC model was found to be 149 percent and 0 percent efficient in terms of the time to settle of rotor angle respond for G2 and G3, respectively, but 394 percent efficient when compared to the uncontrolled model. The decreased settling time values ensured the proposed NFC model's efficacy in damping down the LFO and achieving superior stability over the two controllers. The proposed NFC model has shown significant performance improvement in both the transient and steady-state areas than when the system was design with the two damping controllers.

The associate editor coordinating the review of this manuscript and approving it for publication was Dazhong Ma.

INDEX TERMS Low frequency oscillations, power system stabilizers, farmland fertility algorithm, interline power flow controller, neuro-fuzzy controller.

ABBREVIATIONS

LFO	Low Frequency Oscillation.
AVR	Automatic Voltage Regulator.
FACTS	Flexible AC Transmission Systems.
GA	Genetic Algorithm.
NFC	Neuro-Fuzzy Controller.
NN	Neural Network.
WSCC	Western System Coordinated.
SVC	Static Var Compensator.
UPFC	Unified Power Flow Controller.
SMIB	Single Machine Infinite Bus.
STATCOM	Static Compensatory.
PID	Proportional Integral Derivative.
PIs	Performance Indices.
DC	Direct Current.
AC	Alternating Current.
MBPSS	Multi-Band PSS.
VSI	Voltage Source Inverter.
PSO	Particle Swarm Optimization.
ANFIS	Adaptive Neuro-Fuzzy Inference System.
FFA	Farmland Fertility Algorithm.
PSS	Power System Stabilizer.
IPFC	Interline Power flow Controller.
SVD	Singular Value Decomposition.
KF	Kalman Filter.
TCSC	Thyristor Controlled Series Capacitors.
VSC	Voltage Source Converters.
IEEE	Institute of Electrical and Electronics Engineers.
SSSC	Static Synchronous Series Compensator.
POD	Power Oscillation Dampers.
MF	Membership Function.
EMs	Electromechanical modes.
ANN	Artificial Neural Network.
FO	Fractional-order.
RBF	Radial Basis Function.

I. INTRODUCTION

In the past, electrical power systems were relatively local and simple [1]. Today's power systems are complex with complicated architecture of the networks of transmission lines that connect generator to substations and load centers [2]. One of the outcomes of this linked network is low frequency oscillations (LFOs) with frequencies ranging from 0.2 to 3 Hz [3]. To better understand the causes of LFOs on power system. The literature [4] explains that, generators and loads are interconnected via a network in a power system, and the generators are operated in synchronization at a fixed system frequency. The power change impacts all other generators in the system if one generators speed deviates from the synchronous speed. When this occurs, the system maintains synchronous speed by taking the appropriate control action, such as changing the exciter or turbine controllers. LFO on the other hand, can occur if the controller's settings or the networks status are insufficient. The high-speed excitation mechanism, in particular, weakens the damping properties of LFOs (used to minimize the loss of synchronizing torque and increase transient stability). However, for the case of impedance-mismatch as reported by [5], In power electronics converters with regulated output voltage, negative incremental input impedance is present, resulting in constant power load behavior. Oscillations and overvoltage may arise as a result of a large number of constant power loads in an electrical system, potentially culminating in a system shutdown. Smaller electrical systems, such as planes, ships, and microgrids, cannot handle a large number of loads with negative input impedance. Small-signal stability is determined by the source to load impedance ratio at any given interface, as it is for both dc and ac systems [1], [6]. When LFOs occurs, the oscillation continues for a while and then goes away, or it increases steadily, causing the system to collapse [3]. A significant fault in the system's performance, such as a three-phase short circuit to the ground or the tripe of a transmission line, might cause the power system to oscillate [7]. Therefore, if power fluctuations cause the collapse of a power system, it can be due to the problem of the stabilization of the angle of the large or small perturbation rotor of the power system [8]. The oscillation of the power system is a term used to describe this type of stability. The North American Power Grid's oscillations were first noticed in October 1964 during the north's network of power testing links to the Southern Power Grid [9]. Power oscillation at a frequency of 0.1 Hz was noticed after the connecting line, and the connecting line was tripped after a time.

Moreover, some cases of power system fluctuation in transmission network of many countries have been observed and reported. Examples include: The Great British power grid experienced power fluctuations on the path from Scotland to England in the late 1970s and early 1980s.

When power transmission is transferred, these oscillations are quite high, according to practical experience. The results of a series of studies conducted in 1980 and 1985 showed that these fluctuations occur when the power transfer level is significantly adjusted and the oscillation frequency of these power fluctuations was 0.5 Hz. The installation of power system stabilizers (PSSs) in numerous power facilities in Scotland effectively addressed this issue [10]. Continuous system fluctuations in Taiwan's power grid were reported in 1984, the damping of power fluctuations was found effectively improved by successfully installing PSSs in selected locations [11]. Power oscillations were the direct cause of the North American WSCC network's demise on August 10, 1996. (with frequencies between 0.2 and 0.3 Hz). Lines and generators were expanded with tripping, eventually leading to the western system coordinated council (WSCC) network becoming four islands. These effect left over 5.7 million

consumers in total blackout for nine hours, resulting in significant economic losses [12].

The installation of supplementary excitation control, also known as PSSs, is used to regulate the volatility of power systems in order to maximize the damping of oscillations and improve the oscillation sustainability of power systems [13]. PSSs are a simple, effective, and cost-efficient technique [14]–[17]. PSSs have been installed in most electric power facilities in several countries so far [18]. Installing PSS, on the other hand, does not necessarily give a convincing solution to the power system volatility problem [19], [20]. The PSSs creates a positive component of phase torque with vetting changes in speed on the rotor, thus removing the negative damping torque effect by providing additional damping [21], [22]. The system is deemed to be stable and the power system has good oscillation damping when the system damping improves fast with a damping ratio larger than 0.1 and if there is a LFOs for a certain period (several seconds to ten seconds) and finally disappears, then the power system has oscillation power, but the damping of volatility is weak [23]. Nowadays, the volatility factor of the weak damping of power system known as electromechanical oscillating modes (EMs). Researchers and power system engineers are looking for a viable alternative to installing additional transmission lines for regulating and utilizing the power system. FACTS (Flexible AC Transmission Systems) and ESS (Energy Storage Systems) are two new developing innovations in power system applications that aim to improve the systems reliability and flexibility [23].

Several PSS may not be able to offer enough damping for power fluctuation dampening. As a result, power system engineers and academics are always seeking for novel PSS alternatives to successfully remove power system volatility [24]. Furthermore, traditional PSSs are built using frequency domain phase correction techniques and are based on a linearized model of the power system, which results in reduced performance and does not ensure good operation over a larger range of operating circumstances [25]. In order to enhance power system stability, several optimization techniques have been utilized in the literature to optimize PSS parameter values [2]. For single machine infinite bus (SMIB) systems, artificial intelligence (AI) techniques such as neural networks and fuzzy systems have been suggested, which has recently been broadened to incorporate multi-machine power systems [26]. Various tuning approaches have been offered to alleviate the disadvantages in intelligent systems. Many heuristic optimization methods, such as particle swarm optimization (PSO), genetic algorithm (GA), evolutionary algorithm (EA), have been developed and effectively used in optimization [26]. However, utilizing traditional PSS to dampen low frequency power oscillations is still a work in progress. Other alternative solutions must be revealed in order to address this problem. However, tuning PSS parameter values is a difficult task which possess heavy optimization process and sometimes the PSSs design solution does not always provide a satisfactory solution [27]. This can make the PSSs design to be re-designed again and again.

The FACTS devices, in addition to PSS, are frequently employed. PSSs controller and FACTS devices are often designed simultaneously to further improve the system's dampening efficiency [28]. An Interline Power Flow Controller (IPFC) FACTS device will be connected to PSSs controller in this investigation to further increase the oscillatory stability of the power system [19]. IPFC stabilizer was recently developed for the control of LFOs, with less attention in its implementation. Indeed, IPFC is a new concept adopted in overcoming and managing specific limitations of power line flow in multiple-line transmission systems [29], [30]. Although so many FACTS device example unified power flow controller (UPFC) has been widely developed as oscillatory stabilizers, very few entries have addressed IPFC [30]. The primary distinction between FACTS and PSS stabilizations is that FACTS stabilizations are generally deployed at the power system's critical transmission line. For example, in two-zone connection lines and long power transmission routes are installed for purposes such as load adjustment and voltage control [28]. Therefore, in certain cases, FACTS stabilizations can be easily implemented and effectively eliminate the volatility of the power system. For this reason, the sustained control of power system fluctuations by FACTS has become the subject of recent research and many researchers have been following it since the 1980s [31]. These FACTS stabilizers techniques are usually designed with the coordination of optimized PSSs on the test systems for effective damping. The major drawback of this procedure is difficulty in developing the dynamic IPFC model in the test systems and involves IPFC coordinated PSSs optimization burden.

PSSs controllers based on artificial intelligence (AI) have become a popular research topic in recent years. These intelligent controllers have the capacity to learn from the environment in which they are used to enhance their performance. The literatures have suggested Fuzzy Logic PSSs (FLPSSs), which can be type-1 fuzzy (T1FLS), type-2 fuzzy (T2FLS), or adaptive fuzzy sliding mode PSS, Neural Network PSSs (NNPSSs), Adaptive Neuro-Fuzzy Inference System PSSs (ANFIS-PSSs) [32] etc. were proposed in the literatures. For the FLPSS was found robust and their lower computation burden. It does, however, have a few bottlenecks, such as the development of membership functions, rule selection, and rule construction, which are often handled by trial and error or by human specialists. As a result, designing it is a difficult and time-consuming process. In the same way as the FACTS stabilizers, AI stabilizers techniques are also designed with the coordination of PSSs on the test systems. Designing the PSS parameters utilizing a strong optimization process has shown to be an efficient approach of running the PSS. As a result, a stabilizer must be developed to replace the usual optimized PSSs and FACTS, removing the need for system PSSs design modeling and complexities.

Thus, this paper proposes a stabilizer using Neuro-Fuzzy Controller (NFC) that can replace the work of PSSs and

provide superior properties than the conventional PSSs and FACTS stabilizers in controlling low frequency oscillations in power system. The main contributions of this paper are:

- A metaheuristic FFA technique is proposed for designing PSSs controller on WSCC IEEE test power system. The main contribution is to design dynamic gain parameters of controller in order to handle the system uncertainties and to enhance the steady state and transient performance indices. A considerable contribution is made in this field to enhance the computational cost and convergence for ill-conditioned system operating under multiple working point.
- An eigenvalue placement index was defined for designing the proposed optimal mode feedback and implemented as an optimization problem using FFA. Unlike the classical mode feedback design techniques which requires a conditional condition, the proposed method employs the single value decomposition (SVD) as an analysis tool to determine the appropriate signals for use in the feedback design process. Main contribution of this includes reduced number of parameters of the state feedback matrix, reduced number of control variables, reduced the design time and considering several work points in the design makes the proposed mode feedback resistant to permanent changes in the system. The proposed mode feedback was evaluated on WSCC test systems.
- Since designing dynamic PSSs control parameters give rise to heavy optimization process also, developing dynamic IPFC model in the test systems give rise to heavy system modelling and involves IPFC coordinated PSSs optimization burden, an efficient robust NFC damping controller was proposed to substitute the optimized PSSs and optimized IPFC on the systems. Since PI and PID controllers require a mathematical model of a plant or are model based controllers, NFC in this case is a model-free design because it only depends on expert information and experience. This is an important feature of this controller. Another significant features is that, the proposed NFC model does not require a mathematical model of the test system to be controlled and is operated independent of coordination with conventional optimized PSSs to avoid optimization burden.

This paper is organized: Section II explains the modeling of IEEE 9-bus system model equipped with IPFC and also, the proposed FFA design implementation. Section III explains the proposed methodology for the NFC design. The simulation results obtained to validate the PSSs design, IPFC design and the proposed NFC design on WSCC test system respectively is discussed in section IV with conclusion and future scope of this work presented in last section.

II. SYSTEM MODEL STUDIED

This section shows the overall structure and methodology applied for this work. Figure 1 shows the framework for overall structure of this study which includes selection of PSSs for power system applications and selecting the intelligent approach for designing the multi-machine PSSs. FFA optimization method was a key player in this research. The three objectives of this study are PSSs design using the FFA method, FFA optimized PSSs with IPFC and the proposed NFC design using the FFA method respectively. First the power system nonlinear dynamic equations are modeled using MATLAB/Simulink software. The dynamic modeling has been validated using numerical simulation on IEEE WSCC three-machine benchmark test power system, has been selected for numerical simulation. A PSSs has been designed optimally using FFA optimization method for the test system. The performance evaluation of the FFA-PSSs controller was compared with existing search methods of PSO and GA for PSSs design.

Then, the methodological procedure for obtaining objectives two which is the dynamic modeling of IPFC will be studied and developed. Power system nonlinear dynamic equations equipped with the IPFC device has been implemented in Simulink environment of MATLAB software and its state Equations have been obtained. FFA-based mode feedback is proposed and designed as a supplementary controller for the IPFC device in order to increase the system damping status. In this optimization problem, the objective function of replacing eigenvalues and preventing their drift to the right-hand side is studied to improve the electromechanical modes (EMs) damping status for a set of conditions using the power systems. The performance and efficiency of the proposed IPFC model was compared with the FFA-PSSs method. Lastly, the methodology for attaining objectives three which is the dynamic modeling of NFC was studied and established in the studied test system. Power system nonlinear dynamic equations equipped with the NFC device has been implemented in Simulink environment of MATLAB software. Then the FFA method was used to determine the NFC control parameters. Unlike the PSSs and IPFC stabilizers, the NFC damping controller implementation execute the LFOs control without a linearized mathematical model of the system as such makes the system less complicated and cumbersome. The performance and effectiveness of the proposed NFC model was compared with the two controllers.

III. SIMULATION RESULTS AND DISCUSSION OBTAINED TO VALIDATE PSSs AND IPFC DESIGN ON WSCC TEST SYSTEM

A. SIMULATION RESULTS OF PSSs USING FFA DESIGN METHOD

This section explains the objectives one methodological process for designing the PSSs system for the WSCC three-machine test system considered in Figure 2. In order to obtain permanent conditions, the power system of the Newton-Raphson power distribution program was implemented [112]. To obtain the systems initial conditions, the power system dynamic equations were solved nonlinearly. Also, using Simulink, the internal system characteristics of

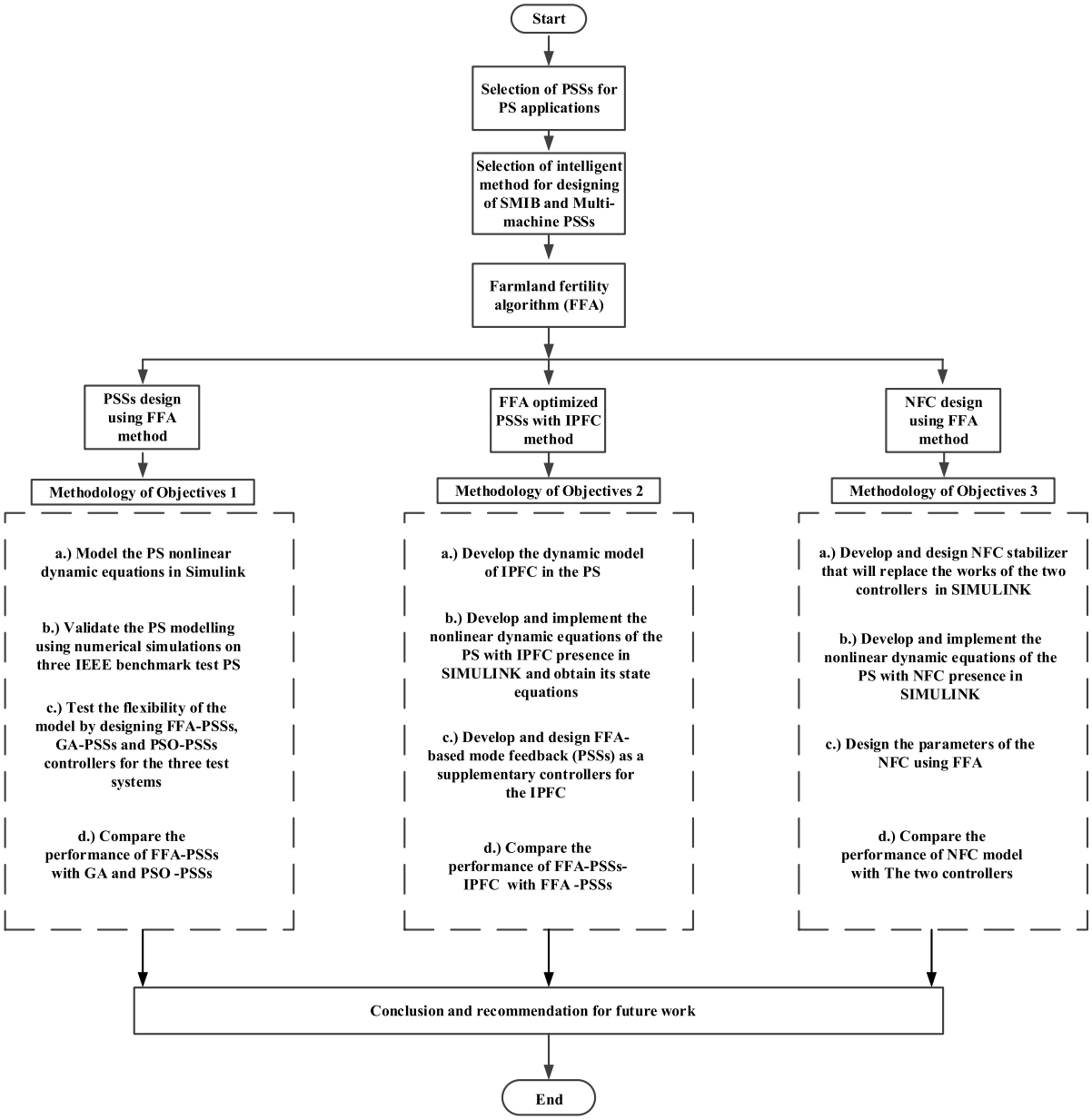

FIGURE 1. Chart representing the overall structure of the work.

the state matrix, eigenvalues, rate of system damping, oscillation frequency and the participation coefficients of the state variables in creating modes were extracted and listed in Table 1.

Based on the results obtained from Table 1, it can be seen that modes 1 and 2 are affected by the speed and angle of the rotor of the second and third generators. Since these modes are caused by rotor angle of the generator, they are called electromechanical mode (EM) and since they are caused by several generators, EM is also called inter-region. Similar arguments can be made for modes 3 and 4. Modes 1 to 4 have a damping ratio of less than 0.1 in terms of the sustainability of low frequency fluctuations are not in a favorable condition and need compensation and control. The results of transient simulations also emphasize on it. Therefore, it is mandatory to add a supplementary controller for this system. Mode number 12 with an eigenvalue equal to zero has appeared in the results. This mode is due to the selection of the angle of the first generator rotor as the reference angle during the implementation of the simulations in this thesis. To improve the damping rate of EMs values to more than 0.1, a damping device called PSS has been installed to the system. Based on the participation coefficients calculated in Table 1, Generator No. 2 has the most effect on EMs, so PSS for this generator is installed. In this study, a speed signal stabilization which is very common has been used. The frequency conversion

TABLE 1. EMs parameters obtained from the linearization of WSCC test system.

Mode Numbers	Eigenvalues	Oscillation Frequency (Hz)	Damping Ratio	Participation Modes
1&2	-0.6856±j12.7756	2.0333	0.0536	$\omega_{2,3}$ $\delta_{2,3}$
3&4	-0.1229±j8.2867	1.3189	0.0148	$\omega_{2,1}$ $\delta_{2,1}$
5&6	-2.3791±j2.6172	0.4165	0.6726	E_{fd1} E'_{q1}
7&8	-4.6706±j1.38750	0.2188	0.9593	$E_{fd2,3}$ $E'_{d2,3}$
9&10	-3.5199±j1.0156	0.1616	0.9608	E'_{q1} E'_{d2} $E_{fd1,2}$
11	-2.1884	0.0	1.0	$E_{fd2,1}$ $E'_{q1,2}$
12	-0.0000	0.0	1.0	$\delta_{1,2,3}$
13	-0.1404	0.0	1.0	ω_1 δ_1
14	-0.8815	0.0	1.0	E'_{q3}
15	-3.2258	0.0	1.0	E'_{d1}

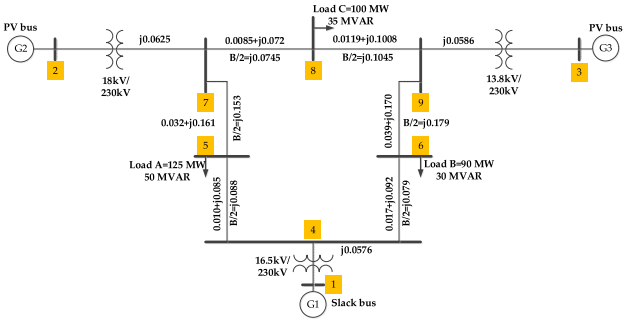

FIGURE 2. WSCC system line diagram [33].

function of this system is given in Equation (1).

$$G(s) = K_G \frac{T_w s\,(1+sT_1)\,(1+sT_3)}{(1+sT_w)\,(1+sT_2)\,(1+sT_4)} \tag{1}$$

The input of which changes are modified is the speed and the output of the voltage that is added to the simulation. In order to facilitate the design of the PSS frequency conversion function is re-written as Equation (2).

$$G(s) = K_G \frac{T_1 T_3}{T_2 T_4} \frac{s\left(s+\frac{1}{T_1}\right)\left(s+\frac{1}{T_3}\right)}{\left(s+\frac{1}{T_w}\right)\left(s+\frac{1}{T_2}\right)\left(s+\frac{1}{T_4}\right)} \tag{2}$$

For this study, the design of PSSs has become an optimization problem and is solved using Farmland Fertility Algorithm (FFA) evolutionary optimization algorithm. In this study, the following optimization model is proposed in Equation (3):

Minimize J

$$J = max\{real(\lambda_i)|\,\lambda_i \in EMs\} + K_P \sum \{real(\lambda_j)|\,real(\lambda_j) > 0\} \tag{3}$$

$$EMs = \left\{(\lambda_k)|\,0 < {}^{im(\lambda_k)}/_{2\pi} < 5\right\} \tag{4}$$

$$K_G^{min} \le K_G \le K_G^{max} \tag{5}$$

$$T_i^{min} \le T_i \le T_i^{max} \tag{6}$$

$$i = 1, \cdots, 4 \tag{7}$$

The first expression in the objective function maximizes the damping of electromechanical and inter-zone modes while the second expression prevents the creation of unstable modes and prevents the drift of eigenvalues to the right hand of the complex zone. The K_P variable is the participation coefficient for creating positive values. During this season simulations, the K_P variable value is 50 and similar to [34] the range of optimization parameters for K_G is [0.001-50], for T_i [0.001-1] was designed for the objective function of a software and simulation was designed using the FFA search algorithm.

B. FFA FOR PSSs DESIGN

Farmers used the FFA search model to divide their farmed area into numerous sections and assess the soil quality in each of these agricultural regions [35]. Each piece of farming area has a particular soil quality that varies. The quality of soil in these agricultural fields is improved by introducing a variety of specific ingredients known as fertilizers. By doing so, the process can be repeated until it reaches a suitable level of quality. It's worth mentioning that the technique for assessing the quality of the labor process and the recovery results at each step is developed using local or national memory, enabling the farmer to select how much repetition and how much addition is chosen in the best quality [36]. The remaining farm regions solutions, i.e. (the lowest quality section of the agricultural areas, the present global memory solutions), are combined with the remainder of the available solutions in the exploration space to enhance outcomes [37]. After each agricultural area altered outcomes using global memory and arbitrary results in the exploration regions, farmers eventually resolved to combine some soil in each farmland portion in terms of the ideal achievable results from its local memory. FFA algorithm is usually broken down into six stages.

Step 1: Population production is determined by the amount of agricultural land sections and the number of solutions accessible in each sector. Equation (8) represents the starting population number.

$$N = k \times n \tag{8}$$

In Equation (8), N signifies the total population of the search area in Equation (8). The number of data points in the optimal problem is denoted by K.

Step 2: After assessing the solutions' applicability and determining each agricultural land portion, all possible search space solutions are adapted.

Step 3: The local and global memories of each section are modified after the solutions for each segment of farmland are determined and combined. To calculate some of the best of each segment's local memory stores, as well as the best of all segment's global memory stores, the quantity of the best local and global memory with statistical relationships is utilized.

Step 4: More changes will occur to the lowest sections, and the solution combination is now in the search area.

Step 5: The knowledge stored in local and global memory is highly suitable to deciding and combining.

TABLE 2. Settings of the FFA optimized variables.

Variables	FFA
k is the number of farmland segment	2
In each farmland portions n is the number of solutions	50
$Npop = k * n$ is the Population number	100
Alpha α	0.6
Beta β	0.4
w	1
Q	0.5
Number of iterations complete	100

TABLE 3. GA pseudo algorithm.

The GA pseudo algorithm [36] **as follows:**
1; determine objective function (OF)
2; assign number of generation $t = 0$ $(t = 0)$
3; randomly create individuals in initial population $P(t)$
4; evaluate individuals in population $P(t)$ using OF
5; while termination criterion is not satisfied do
6; $t = t + 1$
7; select the individuals to population $P(t)$ from $P(t-1)$
8; change individuals of $P(t)$ using crossover and mutation
9; evaluate individuals in population $P(t)$ using OF
10; end while
11; return the best individual found during evaluation

TABLE 4. PSO pseudo algorithm.

The PSO pseudo algorithm [36] **as follows:**
Input: Randomly initialized position and velocity of Particles:
Xi (0) and *Vi* (0)
Output: Position of the approximate global minimum X^*
1: **while** terminating condition is not reached do
2: **for** *i* = 1 to *number of particles* **do**
3: Calculate the fitness function *f*
4: Update personal best and global best of each particle
5: Update velocity of the particle using Equation 2
6: Update the position of the particle using equation 1
7: **end for**
8: **end while**

Step 6: The best solution is to evaluate the various solutions, determine your level of fitness, and keep working continuously.

The relevant FFA techniques parameters for the algorithm are described in Table 2. These characteristics let the sought technique achieve a high rate of convergence and a low computational load [38]. The search model was terminated after a certain number of iterations, and it is commendable to note that the PSS design approach was established and ran several times until the optimum PSSs characteristics were determined [39].

FFA with a primary population of 50 and a repeat number of 100 was executed. Table 3, 4 and 5 shows the three optimization pseudo algorithms for better understanding of their differences.

TABLE 5. FFA pseudo algorithm.

The FFA pseudo algorithm [38] **as follows:**
1: **Input:** problem dimensions(*D*), objective function *f*, optimization limits
2: \\Initialization
3: Initial parameters $n, k, Q, \alpha, \beta, \omega$
4: Let *Soil* be the set of soil sample $X_1, X_2, \dots, X_N$ $Soil = \begin{bmatrix} X_1 \\ X_2 \\ \cdot \\ \cdot \\ \cdot \\ X_N \end{bmatrix}$ X_i *is soil sample*
5: **for** each soil sample in *Soil* **do**
6: To the soil sample area, assign a random real number between [*lb*, *ub*]
7: Calculate the cost of placing a soil sample $X = [X.cost \quad X.position]$
8: **end for**
9: Assign *n soil sample randomly* from *Soil* for each section *j* $Soil = \begin{bmatrix} Section_1 \\ Section_2 \\ \cdot \\ \cdot \\ \cdot \\ Section_k \end{bmatrix}$, $Section_j = [X_1, X_2, \dots, X_n]$
10: **for** each of *Section k* **do**
11: Calculate each section average fitness and local mem , $Section = [Section.localMem]$
12: **end for**
13: \\iterations
14: **while** (the stopping criterion is not met) **do**
15: **for** each of *Section k* **do**
16: Calculate local mem size and Assign population
17: Calculate each section mean fitness
18: **end for**
19: Calculate global mem size and Assign population
20: Get Worst section $Maximum\ fitness\ in\ Sections = Section_{worst}$
21: **for** each of *n in* $Section_{worst}$ **do**
22: Calculate new soil sample for X_{worst} in $Section_{worst}$, $Xnew = h * (X_{ij} - X_{MGlobal}) + X_{ij}$
23: **if** $X_{new} < X_{worst}$
24: $X_{worst} = X_{new}$
25: **end if**
26: **end for**
27: **for** each of *n in* $othersection$ **do**
28: *Calculate new soil sample for other section,* $Xnew = h * (X_{ij} - X_{uj}) + X_{ij}$
29: **if** $X_{new} < X_{othersection}$
30: $X_{othersection} = X_{new}$
31: **end if**
32: **end for**
33: **for** each of soil sample X_i in $Soil$ **do**
34: **if** Q > $rand$
35: *Calculate new soil sample for* X_i, $X_{new} = X_{ij} + \omega * (X_{ij} - Best_{Global}(b))$
36: **if** $X_{new} < X_i$
37: $X_i = X_{new}$
38: **end if**
39: **else**
40: *Calculate new soil sample for* X_i ,$X_{new} = X_{ij} + rand(0.1) * (X_{ij} - Best_{Local}(b))$
41: **if** $X_{new} < X_i$
42: $X_i = X_{new}$
43: **end if**
44: **end if**
45: **end for**
46: $\omega = \omega * R_v$ $0 < R_v < 1$
47: **end** while
48: \\the final stage
49: return the best found value

Figure 3 explains the optimization structure of obtaining the optimal PSSs parameters using the three optimization techniques. Table 6 provides the PSSs optimal parameters

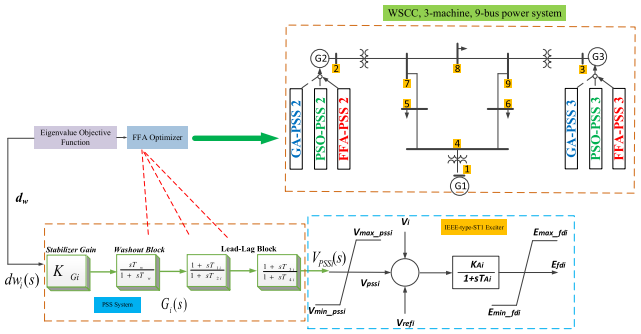

FIGURE 3. GA, PSO and FFA implementation block figure for optimal PSSs design.

TABLE 6. WSCC GA, PSO and FFA optimal PSSs parameters.

Generator	Algorithms	K_G	T_1	T_2	T_3	T_4
G2	GA	2.5229	0.5061	0.0173	0.8007	0.0247
	PSO	4.7686	0.2605	0.0267	0.9220	0.0130
	FFA	3.1490	0.6577	0.0166	0.9622	0.0259
G3	GA	4.3078	0.4769	0.0208	0.6110	0.0226
	PSO	0.8432	0.1898	0.0183	0.6756	0.0225
	FFA	0.6395	0.8330	0.0221	0.5589	0.0171

TABLE 7. Parameters obtain from FFA-PSSs design of WSCC test system.

Mode Number	Eigenvalues	Oscillation Frequency (Hz)	Damping Ratio	Participation Modes
1&2	-4.0720±j13.1963	2.1417	0.3200	$\omega_{2,3}$ $\delta_{2,3}$
3&4	-4.4351±j7.3550	1.2706	0.4442	$\omega_{2,1}$ $\delta_{2,1}$

while Table 7 illustrates the system eigenvalues obtained for the WSCC test system via the FFA method.

To analyze the simulation work of WSCC, the linearization of the system from Table 1, first the dynamic model of power system was developed in MATLAB/Simulink software. An optimal method for the PSSs design is proposed to prevent the drift of eigenvalues to the right during the design and by increasing the damping of oscillations, the system will be lowered to a favorable condition in terms of the sustainability of frequency fluctuations. Based on the participation coefficients calculated in Table 1, the second generator was selected as the suitable place for installing PSS. According to Table 1, the minimum damping for EMs is 0.0148 for modes 3 and 4. By installing optimal PSS in the second generator location, this index was impressively improved to 0.3200 for the desired modes. As can be seen, this index has improved dramatically.

Figure 4 shows the PSS design convergence index comparing FFA, GA, and PSO. The rate of convergence for the FFA was determined to be quicker at 41 iterations than the GA and PSO convergence.

Several potential operating conditions on the test system were examined to satisfy the research objectives. For the first objective, there will be two cases considered for the WSCC test systems. They are:

Case 1: Three-phase symmetric fault at bus 9 were applied to the system for 100 milliseconds in one second with no change in system loading.

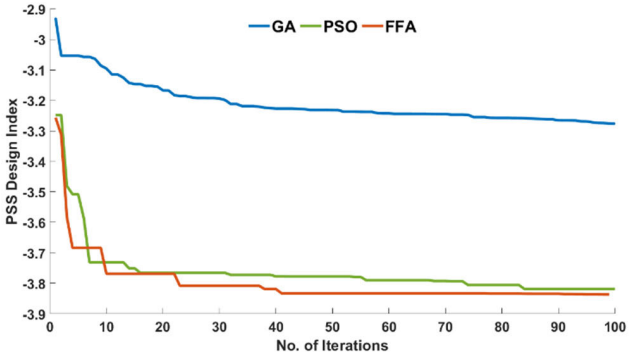

FIGURE 4. PSSs design convergence index comparing FFA with GA and PSO [39].

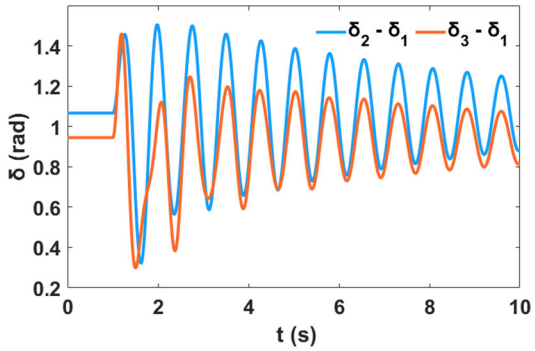

FIGURE 5. Uncontrolled angle of generator 2 and 3 relative to generator 1 for case 1.

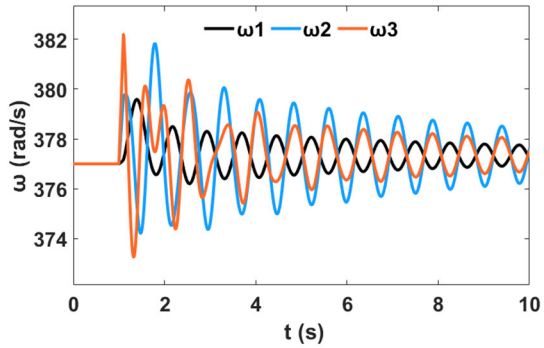

FIGURE 6. Uncontrolled generator speed for case 1.

Case 2: For 100 milliseconds in one second, an adjustment of 5% increments were applied to the third generator excitation voltage reference.

Case 1 Without FFA Controller: The efficiency of FFA-based PSSs design techniques was compared to PSO and GA-based PSSs design methods as follows. The uncontrolled generator 2 rotor angle δ_2 relative to δ_1 ($\delta_2 - \delta_1$) and the uncontrolled generator 3 rotor angle δ_3 relative to δ_1 ($\delta_3 - \delta_1$) is presented in Figure 5 while the uncontrolled speed of the three generators are displayed in Figure 6. These results are consequences of no PSSs installed in the systems.

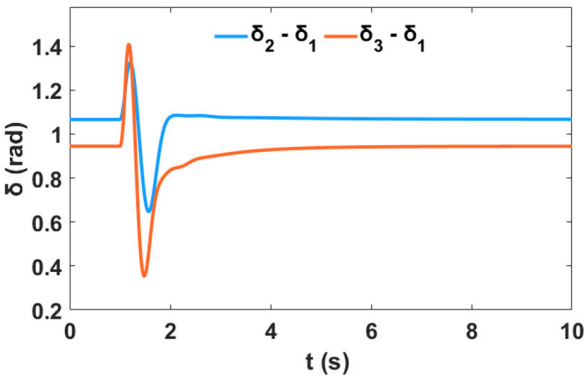

FIGURE 7. Controlled rotor angle changes for case 1.

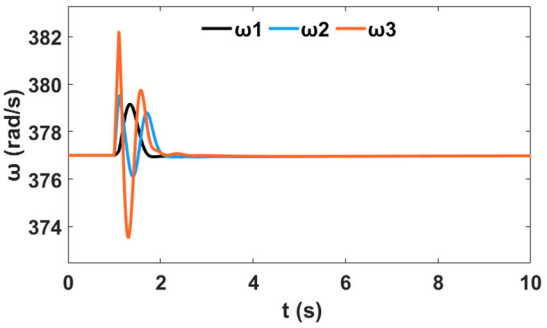

FIGURE 8. Controlled changes in the speed of generators for case 1.

Several Using the FFA, GA, and PSO developed PSSs controllers, several time domain simulations were run to evaluate the power system's performance.

Case 1 With FFA Controller: The controlled generator 2 rotor angle δ_2 relative to δ_1 $(\delta_2 - \delta_1)$ and the controlled generator 3 rotor angle δ_3 relative to δ_1 $(\delta_3 - \delta_1)$ is presented in Figure 7 while the controlled speed of the three generators are displayed in Figure 8. These outcomes are the result of PSSs FFA-based design method.

The optimization issue was addressed and controller settings were found using the FFA method. The FFA-based PSSs approach decreases low frequency fluctuations and enhances the damping ratio of local EMs more effectively than the GA and PSO-based PSSs, according to simulation findings on the WSCC three-machine power system.

Case 2 Without FFA Controller: The uncontrolled generator 2 rotor angle δ_2 relative to δ_1 $(\delta_2 - \delta_1)$, the uncontrolled generator 3 rotor angle δ_3 relative to δ_1 $(\delta_3 - \delta_1)$ and the uncontrolled speed of the three generators are shown in the sequence of Figures 9, 10, and 11 respectively.

Case 2 With FFA Controller: Following the FFA-based PSSs design, controlled generator 2 rotor angle δ_2 relative to δ_1 $(\delta_2 - \delta_1)$, the controlled generator 3 rotor angle δ_3 relative to δ_1 $(\delta_3 - \delta_1)$ and the controlled speed of the three generators are illustrated in the sequence of Figures 12, 13, and 14 respectively.

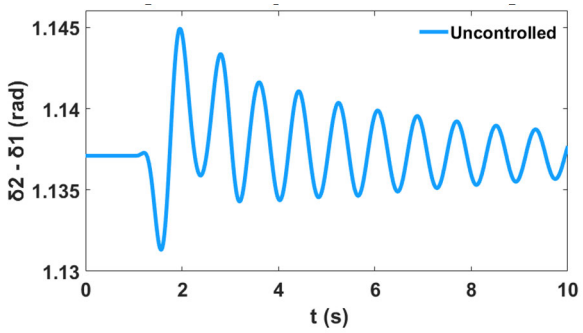

FIGURE 9. For case 2, Uncontrolled generator 2 angle of relative to generator 1.

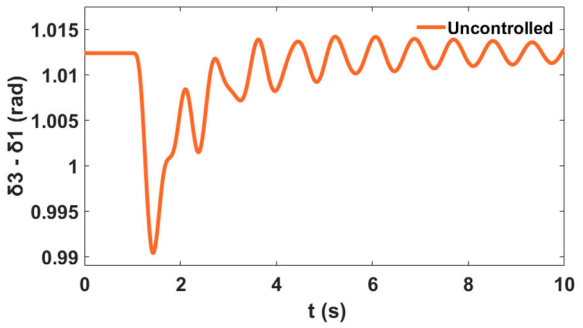

FIGURE 10. For case 2, Uncontrolled generator 3 angle of relative to generator 1.

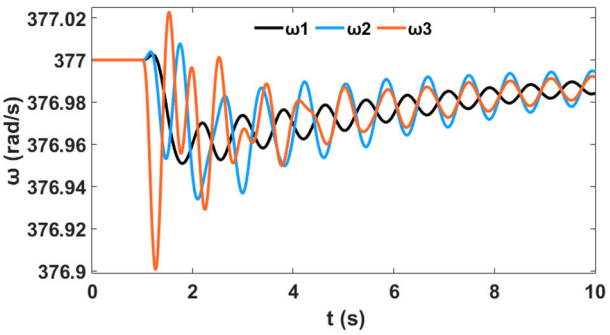

FIGURE 11. Uncontrolled generator speed for case 2.

C. QUANTITATIVE PERFORMANCE EVALUATION COMPARISON FOR PSSs DESIGN

The findings based on the suggested model are compared to the reference results [40] to demonstrate the efficacy of the proposed strategy in contrast to previous approaches. PSSs are used in this reference to enhance the dampening of power fluctuations for generators 2 and 3. Table 8 compares the findings of the proposed model with the reference model [40] in terms of EM damping in a three-machine power system. In this example, the eigenvalues and minimum damping ratio in Table 9, which includes the suggested model, and the literature published models in [40] with the same operating conditions, were gathered for comparison purposes.

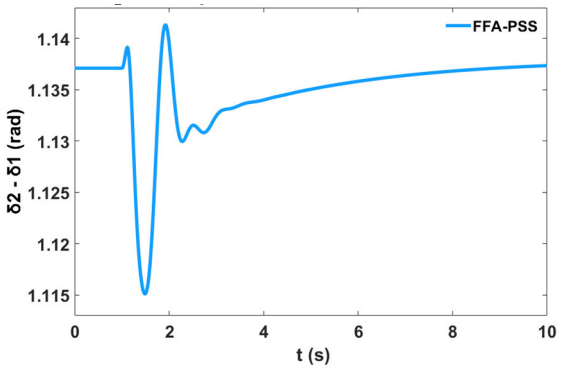

FIGURE 12. For case 2, the controlled generator 2 angle relative to generator 1.

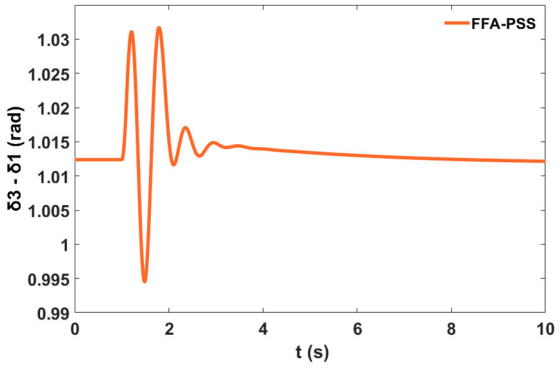

FIGURE 13. For case 2, the controlled generator 3 angle relative to generator 1.

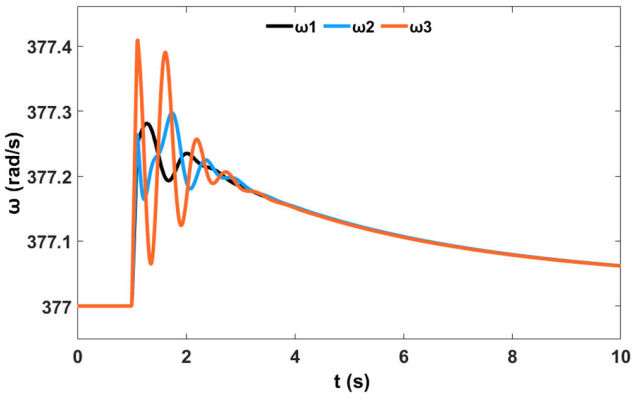

FIGURE 14. Controlled changes in the speed of generators for case 2.

The suggested technique lowers the damping of EMs generated by generators 2 and 3 from 0.0536 to 0.3200 and 0.0148 to 0.4442, respectively, as shown in Table 4.8. In other words, compared to the uncontrolled condition, it enhances damping by 497% and 96.6%, respectively, and by 17.9% and 127.7%, respectively, compared to the reference approach [40]. Both the referenced and constructed models had higher damping ratios than the uncontrolled model. The greater damping ratio value ensured the

TABLE 8. WSCC system PSSs optimized parameters.

Parameters Model	FFA-PSS Model		Reference Model [40]	
	FFA-PSS2	FFA-PSS3	PSO-PSS2	PSO-PSS3
K_G	3.1490	0.6395	8.2250	6.0820
T_1	0.6577	0.8330	0.2010	0.6310
T_2	0.0166	0.0221	0.0500	0.0500
T_3	0.9622	0.5589	0.1370	0.6290
T_4	0.0259	0.0171	0.0500	0.0500

TABLE 9. WSCC system EMs and damping ratio comparison.

Methods	EMs	Damping Ratio
Uncontrolled	-0.6856±j12.7756	0.0536
	-0.1229±j8.2867	0.0148
Proposed	-4.0720±j13.1963	0.3200
	-4.4351±j7.3550	0.4442
Reference [40]	-3.7130±j8.7600	0.3910
	-3.7400±j18.7700	0.1950

TABLE 10. WSCC transient action of first generator for case 1.

Methods	Rotor Speed	
	Settling Time (s)	Rise Time (s)
Uncontrolled	9.98	0.0857
GA-PSS Controlled	2.46	74e-4
PSO-PSS Controlled	1.90	69e-4
FFA-PSS Controlled	1.72	108e-4

TABLE 11. WSCC transient action of second generator for case 1.

Methods	Rotor Speed		Rotor Angle	
	Settling Time (s)	Rise Time (s)	Settling Time (s)	Rise Time (s)
Uncontrolled	9.99	0.019	9.91	0.029
GA-PSS Controlled	2.32	9.1e-4	3.05	69e-4
PSO-PSS Controlled	2.29	9.0e-4	3.03	70e-4
FFA-PSS Controlled	2.04	10e-4	3.14	80e-4

suggested model's effectiveness in dampening down the LFO and achieving superior stability over the conventional model.

In addition, a transient response study for FFA-based PSSs was performed in comparison to GA and PSO-based PSSs. When the system is uncontrolled, this analysis compares the performance of the FFA-based PSSs to the GA and PSO-based PSSs, as well as the three optimized PSSs techniques. For uncontrolled, PSO, GA-based PSS, and FFA-PSS conditions, Table 10 examines how the first machine reacts to a brief disturbance based on system time to settle in seconds and time to rise in seconds. When the FFA-based PSS design is employed, the rotor speed for G1 is increased by a whopping 82.68 percent. This improvement is based on the time it takes for the system to settle in contrast to when it is uncontrolled. Because G1 is the reference machine, the rotor angle response of G1 is zero. Table 11 shows that the time to settle for rotor speed G2 using FFA was improved by 79.48 percent when compared to when the system is uncontrolled, while Table 12 shows that the time to settle for rotor speed G3 using FFA was improved by 79.70 percent when compared to when the system is uncontrolled.

TABLE 12. WSCC transient action of third generator for case 1.

Methods	Rotor Speed		Rotor Angle	
	Settling Time (s)	Rise Time (s)	Settling Time (s)	Rise Time (s)
Uncontrolled	9.98	0.01	9.89	0.016
GA-PSS Controlled	2.39	2.5e-4	4.30	0.15e-4
PSO-PSS Controlled	2.42	2.4e-4	4.31	0.45e-4
FFA-PSS Controlled	2.02	2.4e-4	4.30	0.5e-4

D. MODELING AND SIMULATION RESULTS OF IPFC USING FFA DESIGN METHOD

The primary goal of power distribution control between lines is to distribute power between lines of the transmission system on which it is installed. Other functions, such as dampening power fluctuations in a power system, can be accomplished utilizing various controls on IPFC at the same time. The dynamic power system model is determined by algebraic-differential equations. Generators and their excitation control systems, as well as IPFC, are related to differential equations. This section looks at the fourth-order generator excitation system as well as the first-order generator excitation system. The mechanical power of generators is considered to be constant [34], [41]. The DC link voltage of its inverters is represented by the differential IPFC equations. Each VSCs are considered as a load, and the line network is used to obtain the Y_{new} equivalent admittance matrix. By absorbing loads in the network as constant impedance and obtaining load voltage, generator currents and injectable currents, IPFC branches will be obtained. Assuming that the generators in the first 1st m are repeatedly in $m+1$ to n and IPFC-related system are also $n+1$ and $n+2$. Then the voltage and current interface will be as follows.

$$\begin{bmatrix} I_G \\ I_L \\ I_{IP} \end{bmatrix} = Y_N \begin{bmatrix} V_G \\ V_L \\ V_{IP} \end{bmatrix}, \quad V_{IP} = V_{se},\ I_{IP} = -I_{se} \tag{9}$$

By absorbing loads as constant impedance to the admittance matrix in relationships (10), (11) and (12) the Y_{new} equivalent admittance will be obtained as:

$$\begin{aligned} M_1 &= Y_G - Y_{GL} Y_L^{-1} Y_{LG} \\ M_2 &= Y_{GIP} - Y_L^{-1} Y_{LIP} \qquad (10) \\ M_3 &= Y_{IPG} - Y_{IPL} Y_L^{-1} Y_{LG} \\ M_4 &= Y_{IP} - Y_{IPL} Y_L^{-1} Y_{LIP} \qquad (11) \\ I_{new} &= Y_{new} V_{new} \\ Y_{new} &= \begin{bmatrix} M_1 & M_2 \\ M_3 & M_4 \end{bmatrix} \\ V_{new} &= \begin{bmatrix} V_G & V_{IP} \end{bmatrix}^T \\ I_{new} &= \begin{bmatrix} I_G & I_{IP} \end{bmatrix}^T \qquad (12) \end{aligned}$$

The relationship between algebraic equations of the network (new admin matrix) and stator equations is formed by defining relationships (13), (14), and (15), and the DAEs equations of the network are entirely solved.

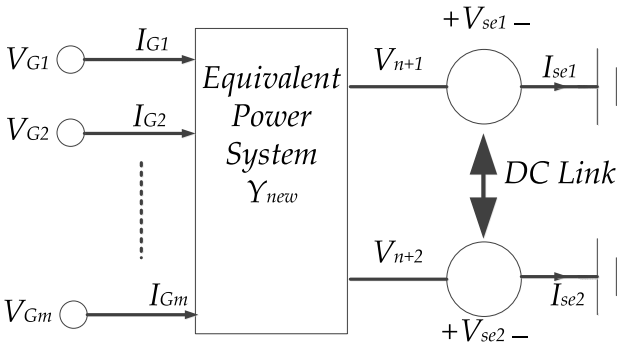

FIGURE 15. Dynamic IPFC model in multi-machine power system.

$$T_M \left(I_d + jI_q\right) = I_G \tag{13}$$

$$T_M \left(V_d + jV_q\right) = V_G \tag{14}$$

$$T_M = diag\left[e^{j(\delta_1 - \frac{\pi}{2})} \ \cdots \ e^{j(\delta_m - \frac{\pi}{2})} \right] \tag{15}$$

Figure 15 shows the test system equipped with IPFC device. Now, by linearization of nonlinear DAEs governing the system behavior, its state equations are obtained as Equation (16).

$$\frac{d\Delta x}{dt} = A\Delta x + B\Delta u \tag{16}$$

$$\Delta y = C\Delta x + D\Delta u \tag{17}$$

The following is a list of vector-based system mode variables:

$$\begin{aligned} x_{IP}^T &= \begin{bmatrix} V_{dc} & x_{PI} \end{bmatrix} \\ x_{pss}^T &= \begin{bmatrix} x_{pss1}^T & x_{pss2}^T & \cdots & x_{pssm}^T \end{bmatrix} \\ x_{pssi}^T &= \begin{bmatrix} x_{p1} & x_{p2} & x_{p2} \end{bmatrix} \end{aligned}$$

A proportional-integral controller (PI) is used to change the voltage of the dc link, hence x_{PI} in the state variables refers to the PI controller mode. Equation (18) considers the transfer function for the PSSs as well as the IPFC supplemental controller in this work. It has five settings that can be changed. The additional pre-phase controller is given as Equation (18):

$$G(s) = K_G \frac{T_w s \left(1 + sT_1\right)\left(1 + sT_3\right)}{\left(1 + sT_w\right)\left(1 + sT_2\right)\left(1 + sT_4\right)} \tag{18}$$

Changes in the generator's normalized angular velocity are regarded the local input signal in the PSS transfer function, and its output is a voltage signal that is added to the generator's stimulation. The IPFC supplementary controller is also considering a similar transfer function. The IPFC controller input can be considered as a combination of local and remote inputs, such as real line power changes and generator speed changes. The output of the supplementary controller can also be applied to each of the IPFC VSCs' amplitude and phase angle inputs.

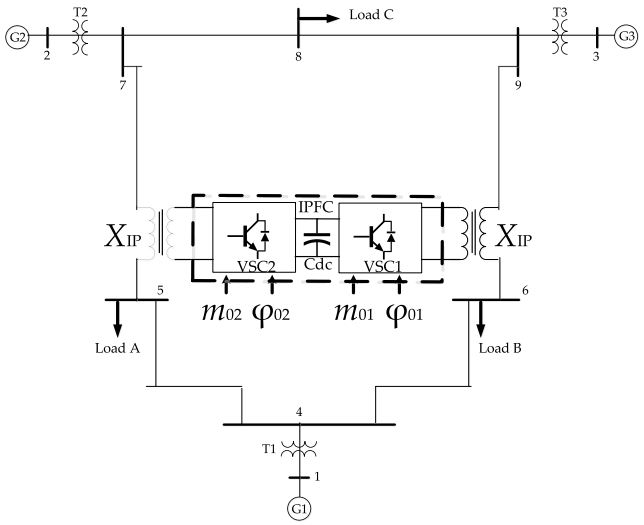

FIGURE 16. WSCC system equipped with IPFC control [29].

PSS and POD design have been turned into an optimization problem in this study, and their parameters were obtained using FFA. The following is the proposed objective function for this optimization problem:

$$J = max\{real(\lambda_i)|\,\lambda_i \in EMs\} + K_P \sum \{real(\lambda_j)|\,real(\lambda_j) \geq 0\} \quad (19)$$

where, $K_{Gpss}^{min} \leq K_{Gpss} \leq K_{Gpss}^{max}$

$$T_{ipss}^{min} \leq T_{ipss} \leq K_{ipss}^{max}$$
$$K_{Gpod}^{min} \leq K_{Gpod} \leq K_{Gpod}^{max}$$
$$T_{ipod}^{min} \leq T_{ipod} \leq K_{ipod}^{max}$$
$$i = 1, \cdots, 4$$

The first statement from the objective function equation increases the damping of electromechanical and inter-zone modes, while the second sentence prevents unstable modes from forming. The K_P variable is an integer coefficient value that is positive and equal to 50. The range of optimization parameters for K_G is considered as [0.001-50] and for T_i as [0.001-1] for PSS and POD respectively [42].

For numerical simulations, the WSCC multi-machine test system was chosen. Simulation of time-domain nonlinearity on the WSCC test system using the IPFC-FFA stabilizer was executed. To find permanent conditions, the system of the Newton-Raphson load distribution program was implemented [43]. To obtain the point of operating, nonlinear equations were solved using Simulink and dynamic equations were linearized and state equations were extracted. Using the extracted state equations, eigenvalues and participation coefficients of all eigenvalues were obtained. EMs in the system are in accordance with Table 13 which shows the EMs of the system without power fluctuations.

With the fast and correct altering of the line power flow with respect to power swings in the system, the system

TABLE 13. EMs of WSCC system without damping power oscillations.

EMs	Damping Ratio	Frequency (Hz)	Participation Modes
-0.8282±j12.7815	0.0647	0.0342	$\delta_{2,3}$ $\omega_{2,3}$
-0.2131±j8.2870	0.0257	1.3189	$\delta_{1,2}$ $\omega_{1,2}$

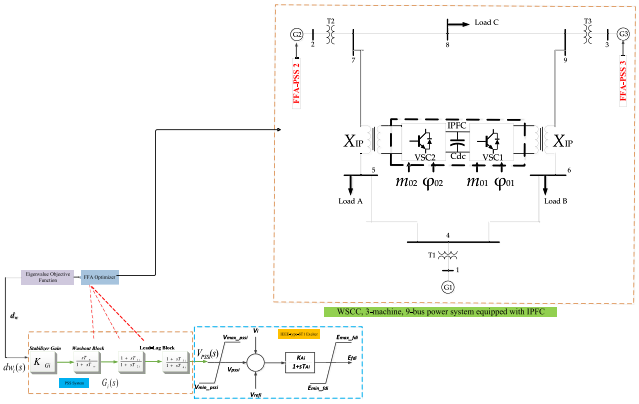

FIGURE 17. FFA implementation block diagram for optimal PSSs and POD design.

stability margin and damping of critical modes are increased [44]. Installation of IPFC with flexible operation and correct series converter control appears to be the best solution to this problem. It is feasible to balance both actual and reactive power of several tie lines between two locations with different lengths using IPFC program [45]. In the power system, the proposed IPFC design is depicted in Figure 16. The IPFC location is chosen based on both static and dynamic objective functions study through detailed load flow and stability analysis [46]. Then, based on the dynamic objective function evaluation, which includes the speed difference of generators and active power oscillations parameters between areas, the best location for stability increase is chosen [46]. The IPFC series converters are best located between buses 5 and 6. An IPFC with two branches is installed in lines 5-7 and 6-9. The control system applied to IPFC is shown in Figure 16. Generators 1, 2, and 3 are responsible for the EMs with the lowest damping ratio, as seen in Table 13. In other words, this system contains a mix of local and inter-regional EMs. To improve the damping profile of these EMs, a PSSs was installed in the generator 2 with a POD on the IPFC installed in line 5-7, according to the existing participation coefficients in Table 13. Similarly, a PSSs was installed in generator 3 with a POD on the IPFC installed in line 6-9, according to the existing participation coefficients Table 13. The good reason for installing the IPFC between line 6 and 9 is because of simplicity of local signal availability compared to the distant signal, only the signal of real power changes passing through line 6-9 is considered as an entry for POD [30]. The second transducer angle modulator's input was supplemented with additional controller output. The proposed objective function was simulated using the FFA algorithm with initial population of

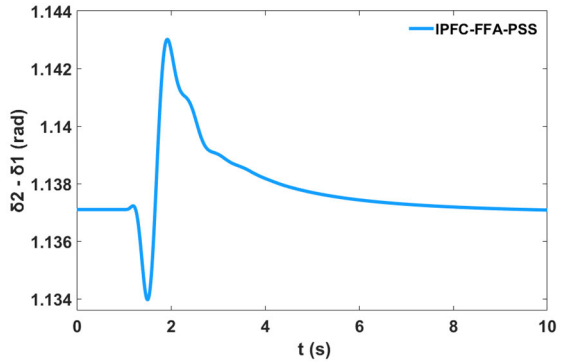

FIGURE 18. For case 1, the controlled angle of generator 2 in relation to generator 1.

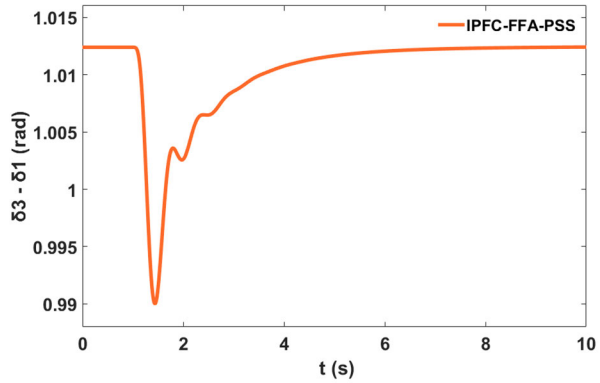

FIGURE 19. For case 1, the controlled angle of generator 3 in relation to generator 1.

50 and number of 100 repetitions, and the PSS and POD values were determined simultaneously. Figure 17 explains the optimization structure of obtaining the optimal PSSs and POD parameters using the proposed FFA optimization technique.

Several potential operating conditions on the test system were examined to satisfy the research objectives. For the second objective, there will be two cases considered for the WSCC test systems. They are:

Case 1: The third generator excitation voltage reference was subjected to small variations of 5% increments for 100 milliseconds in one second.

Case 2: Three-phase symmetric fault at bus 9 were applied to the system for 100 milliseconds in one second with no change in system loading.

Case 1 IPFC-FFA-PSS Controller: The controlled generator 2 rotor angle δ_2 relative to δ_1 ($\delta_2 - \delta_1$), the controlled generator 3 rotor angle δ_3 relative to δ_1 ($\delta_3 - \delta_1$) and the controlled speed of the three generators are illustrated in the sequence of Figures 18, 19, and 20 respectively. These results are the outcome of the system's IPFC-based FFA stabilizer being installed.

Case 2 With IPFC-FFA-PSS Controller: Following the IPFC-FFA-based PSSs design, controlled generator 2 rotor angle δ_2 relative to δ_1 ($\delta_2 - \delta_1$), the controlled generator 3 rotor angle δ_3 relative to δ_1 ($\delta_3 - \delta_1$) and the controlled

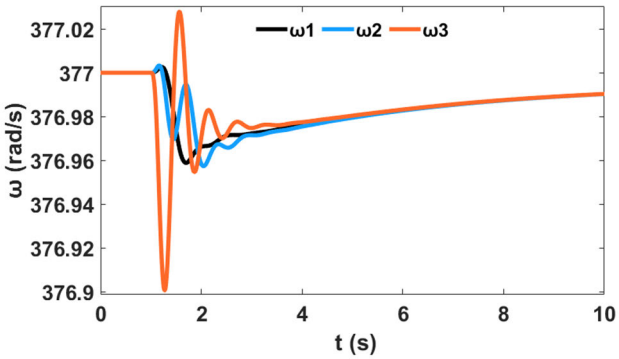

FIGURE 20. Controlled changes in the speed of generators for case 1.

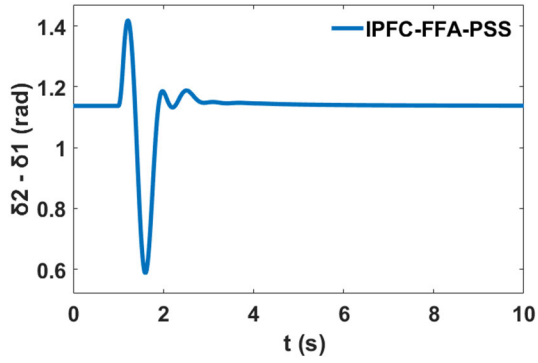

FIGURE 21. For case 2, the controlled angle of generator 2 in relation to generator 1.

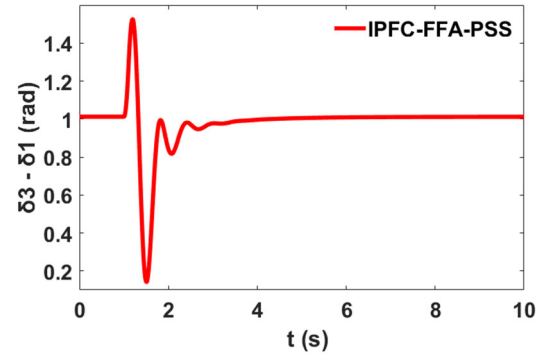

FIGURE 22. For case 2, the controlled angle of generator 3 in relation to generator 1.

speed of the three generators are illustrated in the sequence of Figures 21, 22, and 23 respectively. The installation of an IPFC-based FFA stabilizer on the system yielded these findings.

The supplemental controller built utilizing FFA was found capable to regulate low frequency fluctuations, according to simulation findings obtained for the validation of IPFC-based FFA stabilizer on the multi-machine test system.

E. QUANTITATIVE PERFORMANCE EVALUATION COMPARISON FOR IPFC DESIGN

The results from the proposed model are compared to the reference results to demonstrate the effectiveness of the proposed technique in contrast to other approaches [47]

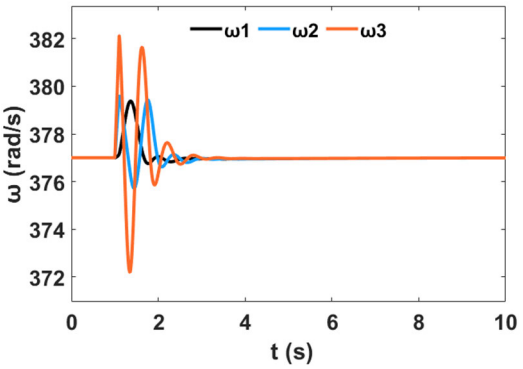

FIGURE 23. Controlled changes in the speed of generators for case 2.

TABLE 14. WSCC system EMs comparison.

Methods	EMs
Uncontrolled Proposed	-0.8282±j12.7815, -0.2131±j8.2870
Uncontrolled Reference model [47]	-0.7075±j11.6065, -0.1864±j7.6324
Controlled Proposed	-5.5223±j11.0058, -2.7320±j11.0687
SVC Controlled Reference model [47]	-2.7345±j9.3101, -0.6607±j7.5522
STATCOM Controlled Reference model [47]	-2.9958±j9.2458, -0.7108±j7.4782
TCSC Controlled Reference model [47]	-2.53±j9.827, -0.7367±j7.6064
SSSC Controlled Reference model [47]	-2.5685±j9.7585, -0.7279±j7.4283
UPFC Controlled Reference model [47]	-2.5131±j9.676, -0.7172±j7.4804

considering operating condition case two. Comparing the results of the proposed model and reference model [47] in the damping of EMs in the three-machine power system is listed in Table 14. The eigenvalues in the Table 14 for three examples, including the proposed model, and the literature published models in [47] with the identical operating circumstances, were gathered in this case for comparative reasons. The reference model utilized Bees search method to optimize the PSS with UPFC, SSSC, TCSC, STATCOM and SVC controls while the proposed model utilized FFA to optimized PSS with IPFC.

The proposed method reduces the damping of EMs caused by the generators. The given eigenvalues for all of the approaches were found on the left half-plane, as shown in the Table 14. Based on this, it can be observed that the proposed method is more effective than current methods. IPFC-based FFA stabilizer was compared with the optimized FFA-based PSSs and when the system is not controlled. A transient response analysis was also carried out for the IPFC's PSS-based stabilizer in comparison to the optimized one. The first machine reacts to momentary disturbance based on the system time to settle in seconds and time to rise in seconds for uncontrolled, FFA-based PSS and IPFC-FFA-PSS circumstances respectively is shown in Table 15. IPFC-FFA-PSS design improves rotor speed G1 transient reaction by an amount of 5.07% and 17.64% respectively. The improvement is based on time to settle and time to rise in comparison to

TABLE 15. WSCC transient action of first generator for case 2.

Methods	Rotor Speed	
	Settling Time (s)	Rise Time (s)
Uncontrolled	9.98	0.085
FFA-PSS Controlled	9.474	0.07
FFA optimized PSS with IPFC Control	1.72	108e-4

TABLE 16. WSCC transient action of second generator for case 2.

Methods	Rotor Speed		Rotor Angle	
	Settling Time (s)	Rise Time (s)	Settling Time (s)	Rise Time (s)
Uncontrolled	9.99	0.019	9.91	0.029
FFA-PSS Controlled	9.45	0.04	3.14	0.002
FFA optimized PSS with IPFC Control	2.04	10e-4	7.83	80e-4

TABLE 17. WSCC transient action of third generator for case 2.

Methods	Rotor Speed		Rotor Angle	
	Settling Time (s)	Rise Time (s)	Settling Time (s)	Rise Time (s)
Uncontrolled	9.98	0.01	9.89	0.016
FFA-PSS Controlled	8.62	0.041	5.70	0.553
FFA optimized PSS with IPFC Control	2.02	2.4e-4	4.30	0.5e-4

when the system is uncontrolled. Similarly, Table 16 shows the time to settle for rotor speed G2 using the IPFC-FFA stabilizer was improved by 5.40% compared to when the system is uncontrolled. Table 17 records an improvement of 13.62% for time to settle of rotor speed G3 using the FACTS stabilizer.

IPFC method controls magnitude and direction of power flow. It's overcome specific limitation of lines, extend the usable transmission limits, enhance grid reliability. No need to check the control or visible power system and reduce number of control variables in the control design problem. The results of numerical simulations show many advantages for the IPFC method. IPFC-based FFA stabilizer design reduces the low frequency fluctuations well and increases the damping ratio of local electromechanical modes in an effective way, according to simulation results. The IPFC device dampens the systems LFOs effectively when coordinated with the optimized PSSs in the system than when there was no coordination. This is a major drawback of the FACTS stabilizer as they require a complementary controller. It makes the system more cumbersome and takes a lot of time to achieve final solution.

IV. PROPOSED NFC METHODOLOGY

This section contains a demonstration of the proposed controller structure and how it was used in this study. To create fuzzy IF-THEN rules and explain membership functions for input and output system parameters, the suggested control

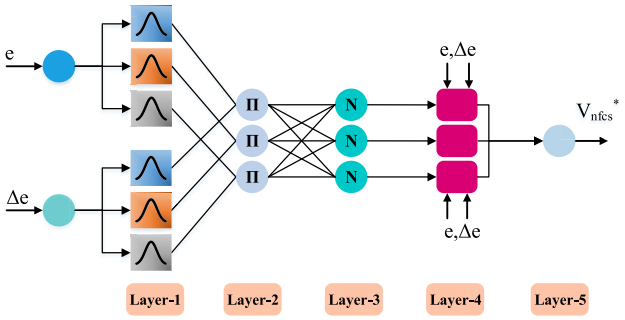

FIGURE 24. Two-input sugeno type NFC assembly.

model was trained from the start [51]. The back-propagation method is used to train this structure, which is essentially a multi-layer NN [13], [33] and [51]. When input-output is provided for training, the back-propagation algorithm measures the system's output and compares it to the preferred output of the training example to illustrate how the neuro-fuzzy system operates. From the output to the entry layer, the error is sent backwards through the device network. When a mistake is communicated, the activation processes of neurons are altered. By differentiating the activation functions of the neurons, the algorithm now calculates the needed changes. The following section looks at the sugeno type's fuzzy laws logical ambiguity [48]:

$$R^j: \ If \ x_1, A^j, \cdots x_n, A_n^j \ then \ y = f_i = a_0^j + k_1^j X_1 + k_2^j X_2 + k_n^j X_n \quad (20)$$

The input and output variables are x and y, respectively.

Figure 24 shows the diagram assembly of the proposed controller in use in the control system [49], [51].

The proposed controller structure's inputs are specified. The (e) and change in error (Δe) inputs of NFC are determined. Layer-1, also known as the Fuzzification layer, selects three Gaussian Membership Functions (MFs) for each input. For Gaussian MF, write the following mathematical expression [13], [51].

$$\sigma_j^1 = exp\left|\frac{\left(x_i - m_{ij}\right)^2}{2\left(\sigma_{ij}\right)^2}\right| \quad (21)$$

where, σ and m present the standard deviation and mean of MF. Firing strengths in the layer-2, also called rule layer, are obtained from membership degrees calculated in the layer-1 as:

$$\sigma_j^2 = \omega_i = \mu_{A_i}(e).\mu_{B_i}(\Delta e) \quad (22)$$

The normalization layer is the third layer, and it determines the normalized firing powers for each rule. The output of this layer is represented by Equation (23).

$$\sigma_j^3 = \bar{\omega}_j = \frac{\omega_j}{\omega_1 + \omega_2 + \cdots + \omega_j} \quad (23)$$

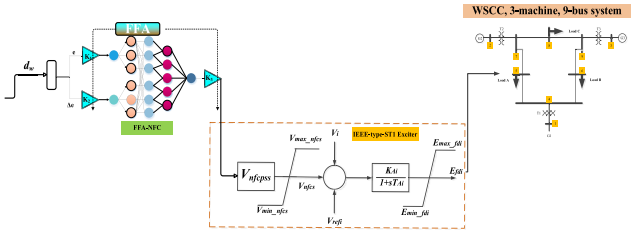

FIGURE 25. Proposed NFC design structure using the FFA method.

The defuzzification layer is the fourth layer, and it computes the rules weighted values for each node as follows:

$$\sigma_j^4 = \bar{\omega}_j f_j = \bar{\omega}_j (k_1 e + k_2 \Delta e + k_0) \quad (24)$$

Here, $(k_1 + k_2 + k_0)$ are the parameter sets. The output layer is labeled layer-5 and is written as follows:

$$\sigma_j^5 = \left(\sum\nolimits_i \omega_i f_i\right) \times \left(\sum\nolimits_i \omega_i\right)^{-1} \quad (25)$$

The squared error (E) in Equation (26) decreases tracking error (e) and is expressed as [48], [51]. In order to update the antecedent and consequent part parameters by backpropagation algorithm, the squared error (E) in Equation (26) lowers tracking error (e) and is expressed as [51]:

$$E = \frac{1}{2}e^2 \quad (26)$$

The following equation can be used to update the parameters of the proposed controller structure if the parameter to be adapted is determined as ϑ.

$$\vartheta(k) = \vartheta(k-1) + \left(-\eta \frac{\partial E(k)}{\partial \vartheta(k)}\right) \quad (27)$$

The variable η is referred to as the learning rate. The partial derivative is calculated using the chain rule [13], [51]. The derivative chain up to the NFC's output is as follows:

$$\delta^1 = \frac{\partial E}{\partial e}\frac{\partial e}{\partial V_{nfcs}^*}\frac{\partial V_{nfcs}^*}{\partial y^6} \quad (28)$$

The FFA algorithm is used to obtain the parameters K_1, K_2, and K_3 in the proposed controller structure as shown in Figure 25.

The NFC scale or control parameters are the names given to these parameters. As a result, a more powerful controller was obtained. The proposed controller receives the machine rotor speed deviation $d\omega$ as an input for controlling the system LFOs. The proposed controller generates a reference signal $\left(V_{nfcs}\right)$. This signal is sent to the excitation system model, which generates the appropriate signals for dampening the system's LFOs.

V. SIMULATION RESULTS AND DISCUSSION OBTAINED TO VALIDATE THE PROPOSED NFC DESIGN ON WSCC TEST SYSTEM

To find the WSCC system working point, nonlinear equations were solved using Simulink, dynamic equations were

TABLE 18. Parameters obtained from the linearization of WSCC test system.

Mode Numbers	Eigenvalues	Oscillation Frequency (Hz)	Damping Ratio	Participation Modes
1&2	-0.6856±j12.7756	2.0333	0.0536	$\omega_{2,3}$ $\delta_{2,3}$
3&4	-0.1229±j8.2867	1.3189	0.0148	$\omega_{2,1}$ $\delta_{2,1}$
5&6	-2.3791±j2.6172	0.4165	0.6726	E_{fd1} E'_{q1}
7&8	-4.6706±j1.38750	0.2188	0.9593	$E_{fd2,3}$ $E'_{d2,3}$
9&10	-3.5199±j1.0156	0.1616	0.9608	E'_{q1} E'_{d2} $E_{fd1,2}$
11	-2.1884	0.0	1.0	$E_{fd2,1}$ $E'_{q1,2}$
12	-0.0000	0.0	1.0	$\delta_{1,2,3}$
13	-0.1404	0.0	1.0	ω_1 δ_1
14	-0.8815	0.0	1.0	E'_{q3}
15	-3.2258	0.0	1.0	E'_{d1}

TABLE 19. Parameters obtained from NFC of WSCC test system.

Mode Numbers	Eigenvalues	Oscillation Frequency (Hz)	Damping Ratio	Participation Modes
1&2	-2.0665±j10.2851	2.0596	0.6194	$\omega_{2,3}$ $\delta_{2,3}$
3&4	-2.4242±j5.2661	1.3704	0.7285	$\omega_{2,1}$ $\delta_{2,1}$
5&6	-1.8669±j3.8200	0.7359	0.8532	E_{fd1} E'_{q1}
7&8	-1.3758±j3.4311	0.2188	0.9001	$E_{fd2,3}$ $E'_{d2,3}$
9&10	-1.8010±j3.6123	0.3707	0.9714	E'_{q1} E'_{d2} $E_{fd1,2}$
11	-2.3040	0.0	1.0	$E_{fd2,1}$ $E'_{q1,2}$
12	-0.0000	0.0	1.0	$\delta_{1,2,3}$
13	-0.2740	0.0	1.0	ω_1 δ_1
14	-0.7394	0.0	1.0	E'_{q3}
15	-3.4057	0.0	1.0	E'_{d1}

linearized, and state equations were extracted. The eigenvalues and participation coefficients of all eigenvalues were calculated using the extracted state equations. The system's EMs are in accordance with Table 18, which characterizes the system's EMs without power fluctuations.

The results in Table 18 show that the speed and angle of the second and third generators' rotors have an effect on modes 1 and 2. These modes are known as electromechanical modes (EM) because they are created by the generator's rotor angle, and they are also known as inter-regional modes since they are caused by many generators. Modes 3 and 4 can be argued in the same way. Modes 1 to 4 have a damping ratio of less than 0.1 in terms of low frequency fluctuations long-term stability, and so require compensation and control. The results of transient simulations also emphasize on it. As a result, a supplemental controller for this system is required. Mode number 12 with an eigenvalue equal to zero has appeared in the results. This mode is due to the selection of the angle of the first generator rotor as the reference angle during the implementation of the simulations in this thesis. NFC damping controller has been added to the system in order to increase the damping rate of EMs to a value greater than 0.1. Generator No. 2 has the greatest effect on EMs, according to the participation coefficients calculated in Table 18, hence NFC is installed for this generator. Table 19 illustrates the new eigenvalues and participation coefficients of all eigenvalues obtained after the WSCC test system was equipped with the proposed NFC stabilizer.

From Table 18, the weak modes of the eigenvalues were increased by a damping ratio greater than 0.1.

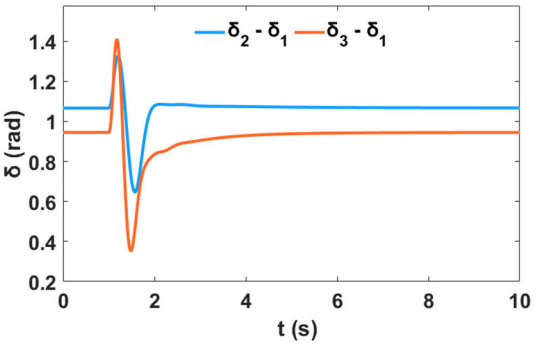

FIGURE 26. Controlled generator rotor angle against the first generator for case 1.

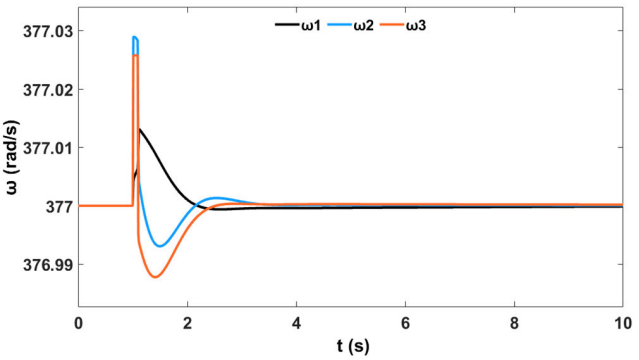

FIGURE 27. Controlled generator speed for case 1.

Several potential operating conditions on the test system were examined to satisfy the research objectives. For the third objective, there will be three cases considered for the WSCC test systems. They are:

Case 1: Three-phase symmetric fault at bus 9 were applied to the system with no change in the system loading.

Case 2: A symmetrical three-phase fault at bus 9 with a 120% increase in active power on generator 2 and generator 3.

Case 3: A symmetrical three-phase fault at bus 9 with an 80% decrease in active power on generator 2 and generator 3.

Case 1 With NFC Controller: The controlled generator 2 rotor angle δ_2 relative to δ_1 ($\delta_2 - \delta_1$) and the controlled generator 3 rotor angle δ_3 relative to δ_1 ($\delta_3 - \delta_1$) is obtainable in Figure 26 while the controlled speed of the three generators are displayed in Figure 27. These outcomes are the result of the NFC stabilizer that was placed in the system.

Case 2 With NFC Controller: A comparative result between the system with uncontrolled, with FFA-PSS controlled and with the proposed NFC controlled was evaluated. The controlled generator 2 rotor angle δ_2 relative to δ_1 ($\delta_2 - \delta_1$), the controlled generator 3 rotor angle δ_3 relative to δ_1 ($\delta_3 - \delta_1$) are explain in Figures 28 and 29 while the controlled generator 2 rotor speed ω_2 relative to ω_1 ($\omega_2 - \omega_1$), the controlled generator 3 rotor speed ω_3 relative to ω_1 ($\omega_3 - \omega_1$) are explained in the order of Figures 30 and 31 respectively.

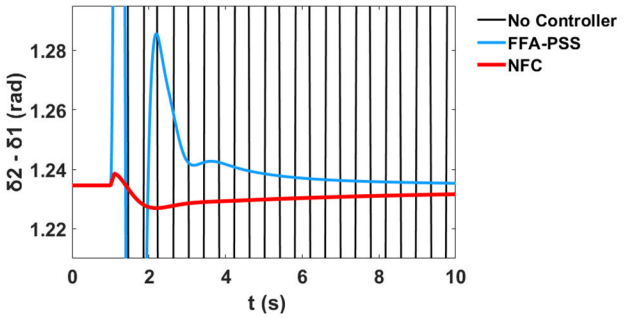

FIGURE 28. For scenario 2, the rotor angle of generator 2 relative to that of generator 1.

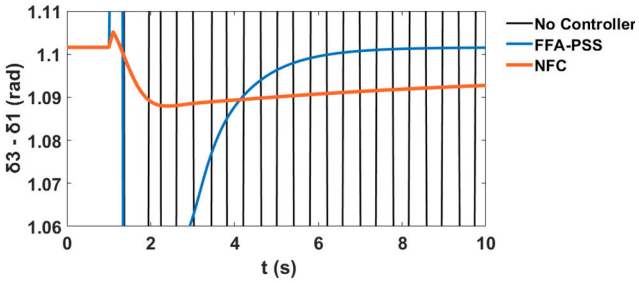

FIGURE 29. For scenario 2, the rotor angle of generator 3 relative to that of generator 1.

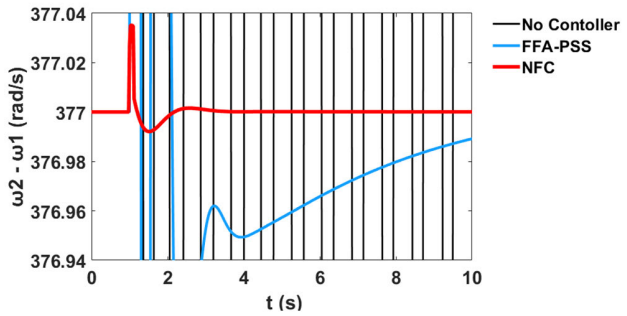

FIGURE 30. For scenario 2, the rotor speed of generator 2 relative to that of generator 1.

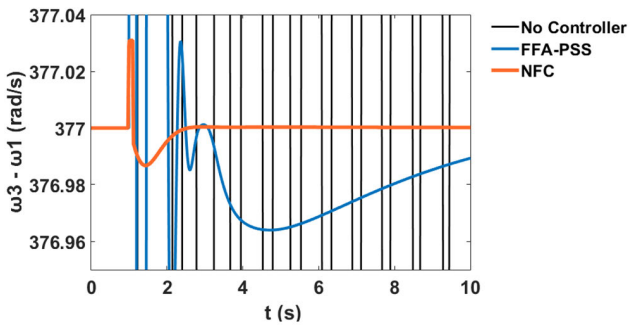

FIGURE 31. For scenario 2, the rotor speed of generator 3 relative to that of generator 1.

These design results were obtained after equipping the system with the proposed NFC stabilizer.

Case 3 With NFC Controller: After installing the NFC model in the system, a symmetrical three-phase fault for 100 milliseconds has been simulated and the results have been

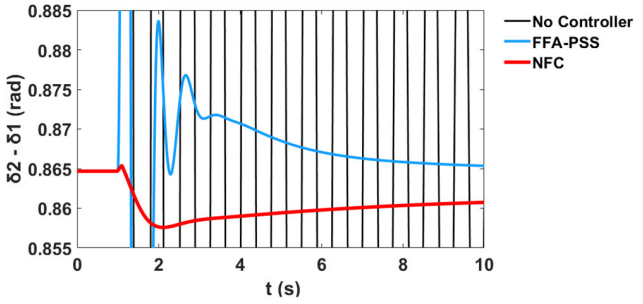

FIGURE 32. For scenario 3, the rotor angle of generator 2 relative to that of generator 1.

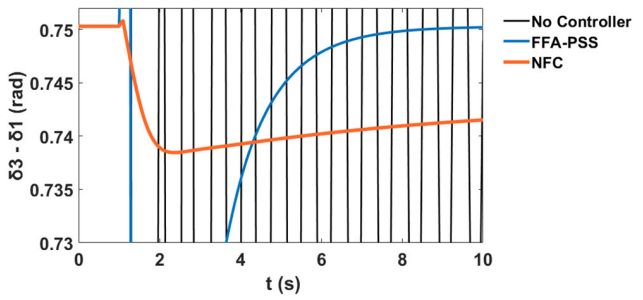

FIGURE 33. For scenario 3, the rotor angle of generator 3 relative to that of generator 1.

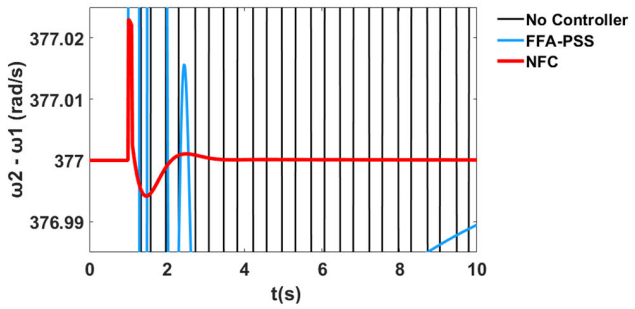

FIGURE 34. For scenario 2, the rotor speed of generator 2 relative to that of generator 1.

obtained. Comparative results show the controlled generator 2 rotor angle δ_2 relative to δ_1 ($\delta_2 - \delta_1$), the controlled generator 3 rotor angle δ_3 relative to δ_1 ($\delta_3 - \delta_1$) are explain in Figures 32 and 33 respectively. The controlled generator 2 rotor speed ω_2 relative to ω_1 ($\omega_2 - \omega_1$) and the controlled generator 3 rotor speed ω_3 relative to ω_1 ($\omega_3 - \omega_1$) are explained in the order of Figures 34 and 35 respectively.

A. QUANTITATIVE PERFORMANCE EVALUATION COMPARISON FOR NFC DESIGN

For the three machines, a transient response study was performed for the proposed NFC stabilizer in comparison to the optimized FFA-based PSSs and when the system is not controlled. For uncontrolled, FFA-based PSS and NFC conditions, Table 20 examines how the first machine reacts to a short disruption based on the system time to settle in seconds

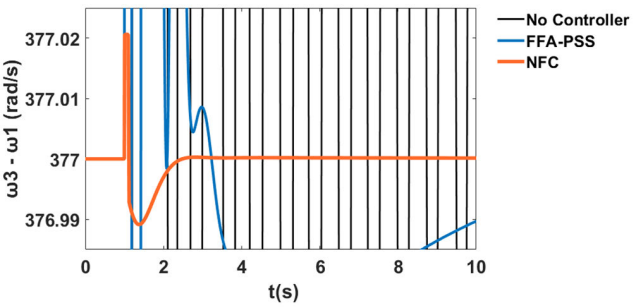

FIGURE 35. For scenario 3, the rotor speed of generator 3 relative to that of generator 1.

TABLE 20. WSCC transient action of first generator for case 1.

Methods	Rotor Speed	
	Settling Time (s)	Rise Time (s)
Uncontrolled	9.98	0.085
FFA-PSS Controlled	3.336	0.030
Proposed NFC Control	1.72	108e-6

TABLE 21. WSCC transient action of second generator for case 1.

Methods	Rotor Speed		Rotor Angle	
	Settling Time (s)	Rise Time (s)	Settling Time (s)	Rise Time (s)
Uncontrolled	9.99	0.019	9.91	0.029
FFA-PSS Controlled	3.03	10e-4	9.44	0.185
Proposed NFC Control	2.04	1e-6	3.14	80e-4

TABLE 22. WSCC transient action of third generator for case 1.

Methods	Rotor Speed		Rotor Angle	
	Settling Time (s)	Rise Time (s)	Settling Time (s)	Rise Time (s)
Uncontrolled	9.98	0.01	9.89	0.016
FFA-PSS Controlled	2.425	2.4e-4	9.34	0.035
Proposed NFC Control	2.02	2e-6	4.30	0.5e-4

and time to increase in seconds. When the NFC stabilizer was employed, the rotor speed G1 transient responsiveness was improved by 66.57 percent in terms of time to settle and 64.70 percent in terms of time to rise. In comparison to when the system is uncontrolled, this improvement is based on time to settle and time to rise. Because G1 was used as the reference machine, the rotor angle response of G1 is zero.

Table 21 shows that the time to settle for rotor speed G2 using the NFC stabilizer was improved by 69.66 percent when compared to when the system is uncontrolled, while Table 22 shows that the time to settle for rotor speed G3 using the NFC stabilizer was improved by 75.70 percent when compared to when the system is uncontrolled.

TABLE 23. WSCC transient performance results comparison for case 1.

Generators	Methods	Rotor speed deviation Settling Time (s)
Generator 2	Uncontrolled	9.99
	FFA-PSS Controlled	3.03
	TLFPSS Control Reference model [52]	3.30
	TLAFPSS Control Reference model [52]	3.10
	Proposed NFC Control	2.04
Generator 3	Uncontrolled	9.98
	FFA-PSS Controlled	2.42
	TLFPSS Control Reference model [52]	3.15
	TLAFPSS Control Reference model [52]	3.10
	Proposed NFC Control	2.02

The results of the proposed model are compared with the results in the reference model [52] to show the effectiveness of the new approach. The reference model [52] examines the design of WSCC PSSs systems utilizing two-level fuzzy PSSs (TLFPSS) and two-level ANFIS PSSs (TLAFPSS). Table 23 compares the numerical results of the proposed model and reference model [52] of G2 and G3 in the damping of EMs in the WSCC test power system for case 1 in the damping of EMs. The reference model [52] has the same operational conditions as the proposal model, which were obtained in this case for comparison purposes. For that specific generator, the technique with lower values of time to settle provides strong stability qualities.

It can be shown from Table 23 that the proposed method minimizes the EM damping caused by the G2 and G3. In other words, it improves the time to settle for EMs generated by the generator 2 by 389 percent when compared to the uncontrolled state, 61.7 percent when compared to the TLFPSS reference model [52], and 51.9 percent when compared to the TLAFPSS reference model [52]. In addition, the suggested model saw a 55.9% and 53.4 percent reduction in settling time for EMs produced by generator 3 when compared to the TLFPSS reference model [52] and the TLAFPSS controlled reference model [52], respectively. On the other hand, the suggested models exhibited effective action on the electric network, placing the eigenvalues in better places than the uncontrolled and referenced models. The reduced settling time values ensured the suggested model's effectiveness in damping down the LFO and achieving improved stability over the reference model.

VI. WSCC TEST SYSTEM QUANTITATIVE PERFORMANCE EVALUATION COMPARISON OF PSS, IPFC, AND NFC DESIGN RESULTS FOR CASE 1

Considering the WSCC system, the effectiveness of the proposed technique in comparison with other approaches for WSCC test system, the quantitative EMs and damping ratio results based on the proposed NFC model are compared with

TABLE 24. WSCC system PSS, IPFC and NFC design results comparison for case 1.

Methods	EMs	Damping Ratio
Proposed FFA-PSS design	-4.0720±j13.1963	0.3200
	-4.4351±j7.3550	0.4442
FFA optimized PSS with IPFC	-5.5223±j11.0058	0.4485
	-2.7320±j11.0687	0.2396
Proposed NFC design	-2.0665±j10.2851	0.6194
	-2.4242±j5.2661	0.7285

the FFA-PSS design results and FFA optimized PSS with IPFC.

Table 24 compares the proposed NFC model's EMs and damping ratio numerical results with the FFA-PSS design results and FFA optimized PSS with IPFC for no change in loading circumstances case 1 in the damping of EMs in the WSCC test power system. For comparison purposes, the FFA-PSS design operating points and FFA optimized PSS with IPFC have identical operating conditions to the proposed NFC model.

VII. SENSITIVITY ON THE APPLICATION OF THE PROPOSED NFC MODEL WITH THE FFA-PSSs AND MULTI-BAND PSSs

Conventional PSSs (CPSS) structures (IEEE PSS2B and IEEE PSS3B) are meant to provide the stabilizing signal by passing only a single frequency band. In this regard, IEEE Std. 421.5 [53] introduced a novel PSS structure called as a multiband PSS (MBPSS). This new MBPSS is unique in that it addresses the three distinct frequency bands for more effective dampening of various power system oscillation types [54], [55]. To establish the NFC stabilizer effects on the improvement of the system dynamic response and the relevance of the proposed FFA optimization method in achieving robustness, a reference model in [56] that studied different number of PSSs was considered. The reference model [56] considers a conventional multi-band PSSs (CMBPSS), a fractional-order (FO) multi-band PSSs (PSO-FO-MBPSS) and a Fractional-order lead-lag compensator-based MBPSS design using a hybrid dynamic GA-PSO method. For WSCC test system, the quantitative EMs and damping ratio results based on the proposed NFC model are compared with the FFA based conventional PSS (FFA-CPSS) design results and the results from the reference model [56].

Table 25 compares the proposed NFC model's EMs and damping ratio numerical results with the FFA-CPSS design results and the results of the reference model [56] for no change in loading circumstances case 1 in the damping of EMs in the WSCC test power system. For comparison purposes, the FFA-CPSS design operating points, the proposed NFC model and that of the reference model [56] have identical operating conditions. From the system eigenvalues and damping ratios of the mechanical mode in Table 25 for normal loading conditions, the proposed NFC model damping rate

TABLE 25. WSCC system CPSS, CMBPSS, PSO-FO-MBPSS, DGA-PSO-FO-MBPSS and NFC design results comparison for case 1.

Methods	EMs	Damping Ratio
Uncontrolled	-0.6856±j12.7756	0.0536
	-0.1229±j8.2867	0.0148
CMPSS [56]	-2.3271±j6.8393	0.3221
	-2.8173±j6.9203	0.3770
FFA-CPSS design	-4.0720±j13.1963	0.3200
	-4.4351±j7.3550	0.4442
PSO-FO-MBPSS [56]	-4.1167±j9.8743	0.3848
	-4.3214±j9.1343	0.4276
DGA-PSO-FO-MBPSS [56]	-4.8706±j8.9743	0.4770
	-5.6326±j10.8141	0.4619
Proposed NFC design	-2.0665±j10.2851	0.6194
	-2.4242±j5.2661	0.7285

values where found 36.73% efficient when compare to the DGA-PSO-FO-MBPSS reference model [56] and 41.30% efficient compared to the PSO-FO-MBPSS model [56]. These values of the damping ratios are significantly improved by the proposed NFC model. It is also clear that the eigenvalues associated with the electromechanical modes have been shifted to the left of the s-plane with the proposed controller compared to the reference model [56] controllers.

VIII. CONCLUSION

In this study, research objectives one was obtained by designing a WSCC multi-machine PSSs system using Farmland Fertility Algorithm (FFA-PSSs controller) and its performance efficiency was compared to GA and PSO-based PSSs controllers. Research objectives two was obtained by adding an Interline Power Flow Controller (IPFC) FACTS device to the PSSs controller to improve the power system's oscillatory stability. The application of the FFA-optimized PSSs with IPFC was achieved in coordinated operation. PSSs optimal design and supplemental controller of power fluctuations for IPFC were conducted out on WSCC multi-machine test systems using a system linear model. Using time-domain simulations and quantitative analysis, the performance and efficiency of the proposed FFA-optimized PSSs with IPFC model was compared to the FFA-PSSs controller. From the simulations and quantitative analysis outcomes, it was found that the coordination of the FFA-optimized PSSs with the IPFC model was found superior than the FFA-PSSs controller in LFOs mitigation. However, in both PSSs design the rise in the computational and simulation costs was found unavoidable. This is a major drawback. To compensate and overcome these drawbacks, this paper proposed a Neuro-Fuzzy Controller (NFC) developed as a damping controller that can take the place of the two controllers. Quantitative analysis results from the WSCC test system simulation show that in terms of settling time G1 rotor speed respond, the proposed NFC model was found to be 480 percent efficient when compared to the uncontrolled model and 0 percent efficient when compared to the FFA-PSS and the FFA optimized PSS with IPFC controller. Similarly, the proposed NFC model

was shown to be 390 percent efficient when compared to the uncontrolled model and 0 percent efficient when compared to the FFA-PSS and the FFA optimized PSS with IPFC controller, respectively, based on the settling time G2 rotor angle response. Furthermore, the proposed NFC model was found to be 216 percent efficient when compared to the uncontrolled model, 0 percent efficient when compared to the FFA-PSSs design technique, and 149 percent efficient when compared to the FFA optimized PSS with IPFC controller. Finally, the proposed NFC model was shown to be 0% efficient when compared to FFA-PSSs and FFA optimized PSS with IPFC controllers, but 394 percent efficient when compared to the uncontrolled model using G3 settling time for rotor speed data. The same goes to the time to settle for the rotor angle respond only the uncontrolled model was found efficient (130%) when NFC model was used with the two controllers 0% efficient. These quantitative simulation outcomes justifies the proposed controllers capacity in substituting the roles of the two damping controllers at the same time overcoming the computational and simulation cost involved when the system is design using the two damping controllers.

REFERENCES

[1] G. L. da Cunha, R. A. S. Fernandes, and T. C. C. Fernandes, "Small-signal stability analysis in smart grids: An approach based on distributed decision trees," *Electr. Power Syst. Res.*, vol. 203, Feb. 2022, Art. no. 107651.

[2] P. Dey, A. Saha, A. Bhattacharya, and B. Marungsri, "Analysis of the effects of PSS and renewable integration to an inter-area power network to improve small signal stability," *J. Electr. Eng. Technol.*, vol. 15, no. 5, pp. 2057–2077, Sep. 2020.

[3] P. Dey, A. Bhattacharya, and P. Das, "Tuning of power system stabilizer for small signal stability improvement of interconnected power system," *Appl. Comput. Informat.*, vol. 16, nos. 1–2, pp. 3–28, Dec. 2017.

[4] K. S. Shim, S. J. Ahn, and J. H. Choi, "Synchronization of low-frequency oscillation in power systems," *Energies*, vol. 10, no. 4, pp. 1–11, 2017.

[5] R. Wang, Q. Sun, W. Hu, Y. Li, D. Ma, and P. Wang, "SoC-based droop coefficients stability region analysis of the battery for stand-alone supply systems with constant power loads," *IEEE Trans. Power Electron.*, vol. 36, no. 7, pp. 7866–7879, Jul. 2021.

[6] W. Bo, D. Boroyevich, R. Burgos, P. Mattavelli, and Z. Shen, "Small-signal stability analysis of three-phase ac systems in the presence of constant power loads based on measured *d-q* frame impedances," *IEEE Trans. Power Electron.*, vol. 30, no. 10, pp. 5952–5963, Oct. 2015.

[7] P. Dey, A. Saha, P. Srimannarayana, A. Bhattacharya, and B. Marungsri, "A realistic approach towards solution of load frequency control problem in interconnected power systems," *J. Electr. Eng. Technol.*, vol. 9, pp. 1–30, Oct. 2021.

[8] J. Zhao, J. Qi, Z. Huang, A. P. S. Meliopoulos, A. Gomez-Exposito, M. Netto, L. Mili, A. Abur, V. Terzija, I. Kamwa, B. Pal, and A. K. Singh, "Power system dynamic state estimation: Motivations, definitions, methodologies, and future work," *IEEE Trans. Power Syst.*, vol. 34, no. 4, pp. 3188–3198, Jul. 2019.

[9] F. Schleif and J. White, "Damping for the northwest—Southwest tieline oscillations—An analog study," *IEEE Trans. Power App. Syst.*, vol. PAS-85, no. 12, pp. 1239–1247, Dec. 1966.

[10] C. M. Gibson, "Application of power system stabilizers on the Anglo–Scottish interconnection—Programme of system proving tests and operational experience," *IEE Proc. C*, vol. 135, no. 3, pp. 255–260, 1998.

[11] Y.-Y. Hsu, S.-W. Shyue, and C.-C. Su, "Low frequency oscillations in longitudinal power systems: Experience with dynamic stability of Taiwan power system," *IEEE Trans. Power Syst.*, vol. PWRS-2, no. 1, pp. 92–98, Feb. 1987.

[12] C. W. Taylor and D. C. Erickson, "Recording and analyzing the July 2 cascading outage [western USA power system]," *IEEE Comput. Appl. Power*, vol. 10, no. 1, pp. 26–30, Jan. 1997.

[13] A. Sabo, N. I. A. Wahab, M. L. Othman, M. Z. A. M. Jaffar, H. Beiranvand, and H. Acikgoz, "Application of a neuro-fuzzy controller for single machine infinite bus power system to damp low-frequency oscillations," *Trans. Inst. Meas. Control*, vol. 43, no. 16, pp. 3633–3646, Dec. 2021.

[14] E. R. Samani, H. Seifi, and M. K. Sheikh-El-Eslami, "A framework for PSS pricing as an ancillary service in a competitive electricity market," *Int. J. Electr. Power Energy Syst.*, vol. 46, pp. 221–227, Mar. 2013.

[15] Y. G. Rebours, D. S. Kirschen, M. Trotignon, and S. Rossignol, "A survey of frequency and voltage control ancillary services—Part II: Economic features," *IEEE Trans. Power Syst.*, vol. 22, no. 1, pp. 358–366, Feb. 2007.

[16] H. Golpîra, M. K. Sheikh-El-Eslami, and H. Seifi, "Power system stabilizer services pricing in an electricity market," *Electr. Power Compon. Syst.*, vol. 43, no. 18, pp. 2050–2058, Nov. 2015.

[17] A. Andreoiu, K. Bhattacharya, and C. Canizares, "Pricing power system stabilisers using game theory," *IEE Proc., Gener., Transmiss. Distrib.*, vol. 152, no. 6, pp. 780–786, 2005.

[18] A. Sabo, N. I. A. Wahab, M. L. Othman, M. Z. A. M. Jaffar, and H. Beiranvand, "Optimal design of power system stabilizer for multimachine power system using farmland fertility algorithm," *Int. Trans. Electr. Energy Syst.*, vol. 30, no. 12, pp. 1–33, Dec. 2020.

[19] T. Guesmi, B. M. Alshammari, Y. Almalaq, A. Alateeq, and K. Alqunun, "New coordinated tuning of SVC and PSSs in multimachine power system using coyote optimization algorithm," *Sustainability*, vol. 13, no. 6, pp. 1–18, 2021.

[20] W. Peres, "Multi-band power oscillation damping controller for power system supported by static VAR compensator," *Electr. Eng.*, vol. 101, no. 3, pp. 943–967, Sep. 2019.

[21] P. S. Kundur, *Power System Stability and Control*. New York, NY, USA: McGraw-Hill, 2004.

[22] P. M. Anderson and A. A. Fouad, *Power System Control and Stability*. Piscataway, NJ, USA: IEEE Press, 2003.

[23] W. Du, H. F. Wang, and R. Dunn, "Power system oscillation stability and control by FACTS and ESS—A survey," in *Proc. 1st Int. Conf. Sustain. Power Gener. Supply (SUPERGEN)*, 2009, pp. 1–13.

[24] X.-P. Zhang, C. Rehtanz, and B. Pal, *Flexible AC Transmission Systems: Modelling and Control*. Berlin, Germany: Springer-Verlag, 2012, pp. 1–26.

[25] S. Gomes, C. H. C. Guimarães, N. Martins, and G. N. Taranto, "Damped Nyquist plot for a pole placement design of power system stabilizers," *Electr. Power Syst. Res.*, vol. 158, pp. 158–169, May 2018.

[26] G. Kasilingam, J. Pasupuleti, C. Bharatiraja, and Y. Adedayo, "Single machine connected infinite bus system tuning coordination control using biogeography: Based optimization algorithm," *FME Trans.*, vol. 47, no. 3, pp. 502–510, 2019.

[27] M. A. Abido and Y. L. Abdel-Magid, "Robust design of multimachine power system stabilisers using Tabu search algorithm," *IEE Proc., Gener., Transmiss. Distrib.*, vol. 147, no. 6, pp. 387–394, 2000.

[28] P. Dey, S. Mitra, A. Bhattacharya, and P. Das, "Comparative study of the effects of SVC and TCSC on the small signal stability of a power system with renewables," *J. Renew. Sustain. Energy*, vol. 11, no. 3, pp. 1–15, 2019.

[29] A. Younesi, H. Shayeghi, and M. Moradzadeh, "Application of reinforcement learning for generating optimal control signal to the IPFC for damping of low-frequency oscillations," *Int. Trans. Electr. Energy Syst.*, vol. 28, no. 2, pp. 1–23, 2018.

[30] M. T. Khosroshahi, F. M. Kazemi, M. R. J. Oskuee, and S. Najafi-Ravadanegh, "Coordinated and uncoordinated design of LFO damping controllers with IPFC and PSS using ICA and SFLA," *J. Central South Univ.*, vol. 22, no. 9, pp. 3418–3426, Sep. 2015.

[31] K. R. Padiyar, *Facts Controllers in Power Transmission and Distribution*. New Delhi, India: New Age International Publication, 2007, pp. 1–548.

[32] S. R. Paital, P. K. Ray, S. R. Mohanty, and A. Mohanty, "An adaptive fractional fuzzy sliding mode controlled PSS for transient stability improvement under different system uncertainties," *IET Smart Grid*, vol. 5, no. 16, pp. 1–15, 2021.

[33] A. Sabo, N. I. A. Wahab, M. L. Othman, M. Z. A. M. Jaffar, H. Acikgoz, and H. Beiranvand, "Application of neuro-fuzzy controller to replace SMIB and interconnected multi-machine power system stabilizers," *Sustainability*, vol. 12, no. 22, pp. 1–42, 2020.

[34] J. H. Chow, M. A. Pai, and P. W. Sauer, *Power System Dynamics and Stability: With Synchrophasor Measurement and Power System Toolbox*, 2nd ed. Hoboken, NJ, USA: Wiley, 2018, pp. 1–364.

[35] H. Zhang, S. Li, and K. Jermsittiparsert, "Optimal design of a proton exchange membrane fuel cell-based combined cooling, heating, and power system by an enhanced version of farmland fertility optimizer," *Energy Sources A, Recovery, Utilization, Environ. Effects*, vol. 42, pp. 1–20, Oct. 2020.

[36] X. Lu, B. Li, L. Guo, P. Wang, and N. Yousefi, "Exergy analysis of a polymer fuel cell and identification of its optimum operating conditions using improved farmland fertility optimization," *Energy*, vol. 216, Feb. 2021, Art. no. 119264.
[37] A. A. Z. Diab, S. I. El-Ajmi, H. M. Sultan, and Y. B. Hassan, "Modified farmland fertility optimization algorithm for optimal design of a grid-connected hybrid renewable energy system with fuel cell storage: Case study of Ataka, Egypt," *Int. J. Adv. Comput. Sci. Appl.*, vol. 10, no. 8, pp. 119–132, 2019.
[38] H. Shayanfar and F. S. Gharehchopogh, "Farmland fertility: A new metaheuristic algorithm for solving continuous optimization problems," *Appl. Soft Comput.*, vol. 71, pp. 728–746, Oct. 2018.
[39] A. Sabo, N. I. A. Wahab, M. L. Othman, M. Z. A. M. Jaffar, and H. Beiranvand, "Farmland fertility optimization for designing of interconnected multi-machine power system stabilizer," *Appl. Model. Simul.*, vol. 4, pp. 183–201, May 2020.
[40] M. A. Abido, "Optimal design of power-system stabilizers using particle swarm optimization," *IEEE Trans. Energy Convers.*, vol. 17, no. 3, pp. 406–413, Sep. 2002.
[41] P. S. Kundur, *Power System Stability and Control*. New York, NY, USA: McGraw-Hill, 2004.
[42] M. Mandour, M. El-Shimy, F. Bendary, and W. M. Mansour, "Damping of power system oscillations using FACTS power oscillation damper—Design and performance analysis," in *Proc. Int. Middle East Power Syst. Conf. (MEPCON)*, 2014, pp. 1–8.
[43] S. Bhowmick, B. Das, and N. Kumar, "An advanced IPFC model to reuse Newton power flow codes," *IEEE Trans. Power Syst.*, vol. 24, no. 2, pp. 525–532, May 2009.
[44] S. R. Paital, P. K. Ray, and A. Mohanty, "Comprehensive review on enhancement of stability in multimachine power system with conventional and distributed generations," *IET Renew. Power Gener.*, vol. 12, no. 16, pp. 1854–1863, Dec. 2018.
[45] V. Azbe and R. Mihalic, "The control strategy for an IPFC based on the energy function," *IEEE Trans. Power Syst.*, vol. 23, no. 4, pp. 1662–1669, Nov. 2008.
[46] E. Gholipour and G. Isazadeh, "Design of a new adaptive optimal wide area IPFC damping controller in Iran transmission network," *Int. J. Electr. Power Energy Syst.*, vol. 53, pp. 529–539, Dec. 2013.
[47] N. A. Arzeha, M. W. Mustafa, and R. M. Idris, "Damping low frequency oscillations via FACTS-POD controllers tuned by bees algorithm," *J. Electr. Eng.*, vol. 17, no. 2, pp. 6–14, 2018.
[48] J. Cervantes, W. Yu, S. Salazar, and I. Chairez, "Takagi–Sugeno dynamic neuro-fuzzy controller of uncertain nonlinear systems," *IEEE Trans. Fuzzy Syst.*, vol. 25, no. 6, pp. 1601–1615, Dec. 2017.
[49] O. F. Kececioglu, H. Acikgoz, C. Yildiz, A. Gani, and M. Sekkeli, "Power quality improvement using hybrid passive filter configuration for wind energy systems," *J. Electr. Eng. Technol.*, vol. 12, no. 1, pp. 207–216, Jan. 2017.
[50] H. Acikgoz, O. F. Kececioglu, A. Gani, C. Yildiz, and M. Sekkeli, "Improved control configuration of PWM rectifiers based on neuro-fuzzy controller," *SpringerPlus*, vol. 5, no. 1, pp. 1–19, Dec. 2016.
[51] J. R. Jang, "ANFIS: Adaptive-network-based fuzzy inference system," *IEEE Trans. Syst., Man, Cybern.*, vol. 23, no. 3, pp. 665–685, May/Jun. 1993.
[52] S. M. Radaideh, I. M. Nejdawi, and M. H. Mushtaha, "Design of power system stabilizers using two level fuzzy and adaptive neuro-fuzzy inference systems," *Int. J. Electr. Power Energy Syst.*, vol. 35, no. 1, pp. 47–56, Feb. 2012.
[53] I. Kamwa, R. Grondin, and G. Trudel, "IEEE PSS2B versus PSS4B: The limits of performance of modern power system stabilizers," *IEEE Trans. Power Syst.*, vol. 20, no. 2, pp. 903–915, May 2005.
[54] D. Rimorov, I. Kamwa, and G. Joós, "Model-based tuning approach for multi-band power system stabilisers PSS4B using an improved modal performance index," *IET Gener., Transmiss. Distrib.*, vol. 9, no. 15, pp. 2135–2143, Nov. 2015.
[55] A. Khodabakhshian, R. Hemmati, and M. Moazzami, "Multi-band power system stabilizer design by using CPCE algorithm for multi-machine power system," *Electr. Power Syst. Res.*, vol. 101, pp. 36–48, Aug. 2013.
[56] H. K. Abdulkhader, J. Jacob, and A. T. Mathew, "Fractional-order lead-lag compensator-based multi-band power system stabiliser design using a hybrid dynamic GA-PSO algorithm," *IET Gener., Transmiss. Distrib.*, vol. 12, no. 13, pp. 3248–3260, Jul. 2018.

ALIYU SABO (Student Member, IEEE) received the bachelor's degree in electrical engineering from Ahmadu Bello University, Zaria, Nigeria, in 2011, and the Master of Engineering degree in power systems engineering from University Putra Malaysia, Malaysia, in 2014, where he is currently pursuing the Ph.D. degree in power systems. Since 2015, he has been working as an Assistant Professor with the Department of Electrical and Electronics Engineering, Nigerian Defence Academy, Kaduna, Nigeria. He is a Registered Engineer under the Council for the Regulation of Engineering in Nigeria (COREN). His research interests include design of robust controllers for power system application, power flow analysis, power system quality, artificial intelligence, and power system stabilizers.

NOOR IZZRI ABDUL WAHAB (Senior Member, IEEE) graduated in electrical and electronic engineering from the University of Manchester Institute of Science and Technology (UMIST), U.K., in 1998. He received the M.Sc. degree in electrical power engineering from Universiti Putra Malaysia (UPM), in 2002, and the Ph.D. degree in electrical, electronic and system engineering from Universiti Kebangsaan Malaysia (UKM), in 2010. He is currently an Associate Professor at the UPM's Faculty of Engineering's Department of Electrical and Electronic Engineering. He is a Researcher at the UPM's Centre for Advanced Power and Energy Research (CAPER) and an Associate Member of the UPM's Centre of Electromagnetic and Lightning Protection Research (CELP). He has over 100 publications to his name (journals: 20 local and 40 international and conference papers: 30 local and 20 international). His research interests include power system stability (both dynamic and control), artificial intelligence applications in power systems, and power system quality. He is a Chartered Engineer with the Engineering Council, U.K., and the Institution of Engineering and Technology (IET), U.K. He is a Professional Engineer (Ir.) with the Board of Engineers Malaysia (BEM) and a member of The Institution of Engineers Malaysia (IEM). He is a member of the IEEE Power and Energy Society (IEEE-PES), the IEEE Computational Intelligence Society (IEEE-CIS), a member of the Institution of Engineering and Technology (IET) U.K., and an International Rough Set Society Member (IRSS).

MOHAMMAD LUTFI OTHMAN (Senior Member, IEEE) received the B.Sc. degree (Hons.) *(Magna Cum Laude)* in electrical engineering from the University of Arizona (UofA), Tucson, Arizona, USA, in 1990, and the M.Sc. and Ph.D. degrees in electrical power engineering from the Universiti Putra Malaysia (UPM), Serdang, Malaysia, in 2004 and 2011, respectively.

He is currently an Associate Professor with the Department of Electrical and Electronics Engineering, Faculty of Engineering, Universiti Putra Malaysia. He is also a Research Member at the Advanced Lightning, Power and Energy Research (ALPER), UPM. He also practices as an Electrical Engineering Consultant in electrical services installation works by diversifying as an electrical director/partner in a local engineering consulting firm. His areas of research interest include, among others, power system protection (protective relay operation modeling and analysis, computational-intelligence-based data mining for knowledge discovery in relay database, application of artificial intelligence in protection algorithms, adaptive numerical protective relays, development of numerical protective relays), power system operation (power quality, smart grid, distributed generation), electrical services installation works (design and project administration consultancy), and energy efficiency management (demand side management, building energy management system).

Dr. Othman is also a Professional Engineer with the Practicing Certification (PEPC) registered under the Board of Engineers Malaysia (BEM), an ASEAN Chartered Professional Engineer (ACPE), a Chartered Engineer (C.Eng.) registered under the Engineering Council U.K., a Professional Technologist (P.Tech.) registered under the Malaysian Board of Technologists, a Registered Electrical Energy Manager (REEM) under Energy Commission Malaysia, a Certified Professional in Measurement and Verification (CPMV) under Malaysian Green Technology Corporation, a Corporate Member of the Institution of Engineers Malaysia (IEM), and a member of the Institution of Engineering and Technology (IET) U.K., the International Rough Set Society (IRSS), the Asian Council of Science Editors (ACSE), the Academic Keys Who's Who in Engineering Higher Education (WWEHE), the International Rough Set Society (IRSS), and a Phi Kappa Phi (FKF) Honor Society, The University of Arizona. His biographical profile is mentioned in the Marquis Who's Who in the World 2016 (33rd Edition). As a Professional Engineer, he is a Mentor and Professional Interviewer for IEM/BEM Professional Engineer as well as the Engineering Council UK Chartered Engineer aspirants and an Engineering Accreditation Council (EAC) Panel Member under BEM.

MAI ZURWATUL AHLAM BINTI MOHD JAFFAR received the B.Sc. degree (Hons.) in mathematics from Universiti Putra Malaysia, Malaysia, and the Ph.D. degree in mathematics from the Division of Mathematics, University of Dundee, Scotland, U.K., in 2013. She worked in various industries before continuing study, including as a Quality Control Assistant in rubber industry and a Research Assistant (RA) at Sumitomo Corporation, Osaka, Japan, in the field of entomology. She is currently a Senior Lecturer at the Department of Mathematics and Statistics, Faculty of Science, UPM. Her main interest includes innovation and creativity associated with teaching. Apart from that, she focuses on data forensics related to biometric data and derivations of algorithm connected to virus–protein cluster network and vascular network system.

HAKAN ACIKGOZ received the Ph.D. degree in electrical and electronics engineering from Kahramanmaras Sutcu Imam University, in 2018.

He is currently employed as an Assistant Professor at the Gaziantep Islam Science and Technology University's Department of Electrical and Electronics Engineering. He has 11 years of experience working in the academic sector. His research interests include power electronic converters, optimization, intelligent controllers, artificial intelligence, and deep learning.

HAMED NAFISI received the B.Sc., M.Sc., and Ph.D. degrees in electrical engineering from the Iranian Center of Excellence in Power Systems, Amirkabir University of Technology, Tehran, Iran, in 2006, 2008, and 2014, respectively. He is currently a Research Fellow with the School of Electrical and Electronic Engineering, Technological University Dublin (TU Dublin). His current research interests include smart grid, peer-to-peer energy trading, electric vehicles, power system protection, and power electronics application in power systems.

HOSSEIN SHAHINZADEH (Member, IEEE) was born in Isfahan, Iran, in 1987. He graduated from the Iranian Center of Excellence in Power Systems, Amirkabir University of Technology (Tehran Polytechnic), Tehran, Iran, with a scientific education in electrical engineering. Since September 2015, he has been an Academic Member of the Islamic Azad University of Najafabad's (IAUN) Department of Power Engineering, Faculty of Electrical Engineering. In Tehran, he works as an Associate Researcher at the Iran Grid Secure Operation Research Institute, AUT, and the Niroo Research Institute (NRI). He is also a Senior Scientist at SMRC, IAUN, Isfahan, where he works in the subject of smart city research. The Internet of Things (IoT), artificial intelligence, metaheuristic optimization methods, big data analytics, blockchain, V2G integration, 5G technology in smart grids, renewable energy deployment, energy storage facilities, power markets, microgrids, and long-term energy planning are some of his research interests in smart grids.